AGU PUBLICATIONS

JGR

Journal of Geophysical Research: Solid Earth

RESEARCH ARTICLE
10.1002/2013JB010431

Key Points:
- We show seismic lines crossing a rift from less to higher rifted crust
- The style of rifting changes from symmetric to asymmetric
- The rift developed W-E, and extension rates increase N-S leading to asymmetry

Correspondence to:
S. Moeller,
stefanmoeller@freenet.de

Citation:
Moeller, S., I. Grevemeyer, C. R. Ranero, C. Berndt, D. Klaeschen, V. Sallares, N. Zitellini, and R. de Franco (2014), Crustal thinning in the northern Tyrrhenian Rift: Insights from multi-channel and wide-angle seismic data across the basin, *J. Geophys. Res. Solid Earth*, *119*, 1655–1677, doi:10.1002/2013JB010431.

Received 12 JUN 2013
Accepted 28 JAN 2014
Accepted article online 5 FEB 2014
Published online 26 MAR 2014

Crustal thinning in the northern Tyrrhenian Rift: Insights from multichannel and wide-angle seismic data across the basin

S. Moeller[1,2], I. Grevemeyer[1], C. R. Ranero[3], C. Berndt[1], D. Klaeschen[1], V. Sallares[4], N. Zitellini[5], and R. de Franco[6]

[1]GEOMAR Helmholtz Centre for Ocean Research Kiel, Kiel, Germany, [2]Now at Petroleum Geo-Services, Oslo, Norway, [3]Barcelona Center for Subsurface Imaging, ICREA at CSIC, ICM, Barcelona, Spain, [4]Barcelona Center for Subsurface Imaging, ICM, CSIC, Barcelona, Spain, [5]Istituto di Scienze Marine ISMAR, CNR, Bologna, Italy, [6]Istituto per la Dinamica dei Processi Ambientali, CNR, Milan, Italy

Abstract Extension of the continental lithosphere leads to the formation of rift basins or rifted continental margins if breakup occurs. Seismic investigations have repeatedly shown that conjugate margins have asymmetric tectonic structures and different amount of extension and crustal thinning. Here we compare two coincident wide-angle and multichannel seismic profiles across the northern Tyrrhenian rift system sampling crust that underwent different stages of extension from north to south and from the flanks to the basin center. Tomographic inversion reveals that the crust has thinned homogeneously from ~24 km to ~17 km between the Corsica Margin and the Latium Margin implying a β factor of ~1.3–1.5. On the transect 80 km to the south, the crust thinned from ~24 km beneath Sardinia to a maximum of ~11 km in the eastern region near the Campania Margin (β factor of ~2.2). The increased crustal thinning is accompanied by a zone of reduced velocities in the upper crust that expands progressively toward the southeast. We interpret that the velocity reduction is related to rock fracturing caused by a higher degree of brittle faulting, as observed on multichannel seismic images. Locally, basalt flows are imaged intruding sediment in this zone, and heat flow values locally exceed 100 mW/m^2. Velocities within the entire crust range 4.0–6.7 km/s, which are typical for continental rocks and indicate that significant rift-related magmatic underplating may not be present. The characteristics of the pre-tectonic, syn-tectonic and post-tectonic sedimentary units allow us to infer the spatial and temporal evolution of active rifting. In the western part of the southern transect, thick postrift sediments were deposited in half grabens that are bounded by large fault blocks. Fault spacing and block size diminish to the east as crustal thinning increases. Recent tectonic activity is expressed by faults cutting the seafloor in the east, near the mainland of Italy. The two transects show the evolution from the less extended rift in the north with a fairly symmetric conjugate structure to the asymmetric margins farther south. This structural evolution is consistent with W-E rift propagation and southward increasing extension rates.

1. Introduction

Extension of the lithosphere controls the evolution of rift basins and conjugate continental margins. Many workers report that conjugate-rifted margins have crustal and tectonic asymmetric structures, including the magma-poor margins in the North Atlantic [*Pérez-Gussinyé et al*., 2003; *Shillington et al*., 2006; *Ranero and Pérez-Gussinye*, 2010] or at basins like the Woodlark Basin [*Taylor et al*., 1995; *Speckbacher et al*., 2011] or in the East Scotia Sea [*Barker and Hill*, 1980]. Conjugate margins differ in crustal thickness or amount of faulting. Moreover, upper crustal extension measured by fault displacements imaged in seismic cross sections often does not match the extension of the crust [*Davis and Kusznir*, 2004; *Reston*, 2005]. A conceptual hypothesis that might explain asymmetric rift structures is the simple shear model [e.g., *Wernicke*, 1985]. It proposes that the crust is separated into an upper and lower part by a crustal scale or even lithospheric-scale detachment fault. Although potential shear zones within the mantle are observed on seismic images [e.g., *Reston*, 1993], their nature and role remain controversial. Potential shallow dipping detachment faults have been detected at the well-surveyed Galicia rifted margin and Porcupine Basin (*S* and *P* reflectors) [e.g., *Reston et al.*, 2004]. However, such features may just be present at large stretching factors of $>$3.5 when the entire crust has become brittle [*Pérez-Gussinyé and Reston*, 2001]. In rifts showing different amounts of extension, e.g., the northern Porcupine Basin, it is reported that the style of rifting changes from symmetric

to asymmetric extension associated with the development of detachment faults cutting under the entire basin [*Reston et al*., 2001]. Alternative models, e.g., for the conjugate margins of Newfoundland and Iberia, propose that faulting changes from coeval in the rift basin stage to sequential during the conjugate margin formation stage [*Ranero and Pérez-Gussinye*, 2010]. This change in faulting style leads to a change from symmetric to asymmetric structures formed by planar Andersonian-type faulting, where no low-angle detachment fault is needed. The sequential development of faulting has been reported from field campaigns in the Suez Rift [*Gawthorpe et al*., 2003]. In most of these models, little is known about the initial conditions prior to rifting, for instance, the crustal thickness or inherited zones of weakness and structures. Similarly, few examples exist documenting the transition from little extended symmetric structures to asymmetric conjugate margin structures within the same rift system. Analog experiments indicate that the pre-rift Moho topography might have an important control on the rift process [*Corti and Manetti*, 2006], where initial asymmetric Moho conditions may lead to asymmetry in the amount of extension accommodated by faults.

We present the comparison of the results of two coincident wide-angle seismic (WAS) lines and prestack time-migrated (PSTM) seismic profiles transecting the northern Tyrrhenian Sea Basin (Figure 1). A detailed explanation of the modeling procedures and interpretation of line AB has been presented by *Moeller et al*. [2013]. In this contribution, we present the crustal scale velocity model and prestack time-migrated seismic images of the line CD and a joint geological interpretation of both seismic transects to understand the spatial evolution of the deformation across the basin (Figure 1).

The triangular shaped and structurally asymmetric Tyrrhenian Basin is located in the western Mediterranean Sea. It is confined by the islands of Corsica, Sardinia, Sicily, and mainland Italy (Figure 1a). The aim of our study is to reveal the sedimentary, tectonic, and crustal velocity architecture by combining both seismic data sets. The Tyrrhenian Basin underwent little stretching in the northern sector, with increasing amount of stretching toward the southeast, where full continental breakup occurred and basalt floor basins and serpentinized mantle peridotite have been drilled (Ocean Drilling Program (ODP) Site 651), [*Kastens et al*., 1987, 1988]. Thus, the basin is an interesting area to study the processes of rifted continental margins as a function of changes in the amount of extension. In this contribution, we have investigated the development of structures that are typically observed at the early stage of rifted continental margin evolution. In particular, we examine the rifting evolution in which the deformation is changing from the early rift phase with about 30% stretching on line AB and no clear asymmetry (*Moeller et al*. [2013] to higher extension on line CD where the margins of the basin display distinct asymmetric crustal features.

2. Geological Setting

The extension creating the basins of the western Mediterranean Sea is the result of trench migration due to the rollback of the Tethys Mesozoic oceanic lithosphere, which subducted the underneath portions of the European plate since late Cretaceous time [*Faccenna et al*., 2001; *Jolivet et al*., 1999]. Tensile stress on the overriding plate triggered the episodic opening of several back-arc basins in the western Mediterranean Sea. In the region of interest, this development began along southern France and Iberia with the drift of the Balearic block, Sardinia, and Corsica away from continental Europe and led to the opening of the Gulf of Lion and the Valencia Trough during Oligocene time ~30 Ma ago [*Rosenbaum et al*., 2002; *Cherchi and Montadert*, 1982]. Extension continued in the Gulf of Lion and the Ligurian Sea during early Miocene time (21-16 Ma [*Faccenna et al*., 2001]) and the Sardinia-Corsica block of European continental crust underwent counterclockwise rotation of 30° to finally collide with the Adriatic foreland.

This event led in the Miocene to the formation of the NW-SE striking Apennine orogenic fold-and-thrust belt, rotating counterclockwise in the Adriatic area [*D'Agostino et al*., 2008]. The ongoing trench migration finally triggered the opening of the Tyrrhenian back-arc basin [*Malinverno and Ryan*, 1986; *Kastens et al*., 1987; *Rosenbaum et al*., 2002] from Tortonian age (9–10 Ma) to early Pliocene (5 Ma) in the northern part of the basin. Rifting migrated toward the southeast where the existence of a subducted slab is indicated by a narrow, NW-SE-directed Wadati-Benioff zone beneath the Calabrian Arc and the active volcanic archipelago of the Aeolian region [*Faccenna et al*., 2001; *Malinverno and Ryan*, 1986]. The rift propagation is also reflected by the age of volcanic rocks. Volcanic rocks have ages of ~30–15 Ma onshore Sardinia and Corsica. Farther east, samples from Elba, Montecristo, and Mount Vercelli have ages of 8–6 Ma and 5–2 Ma on Giglio Island or

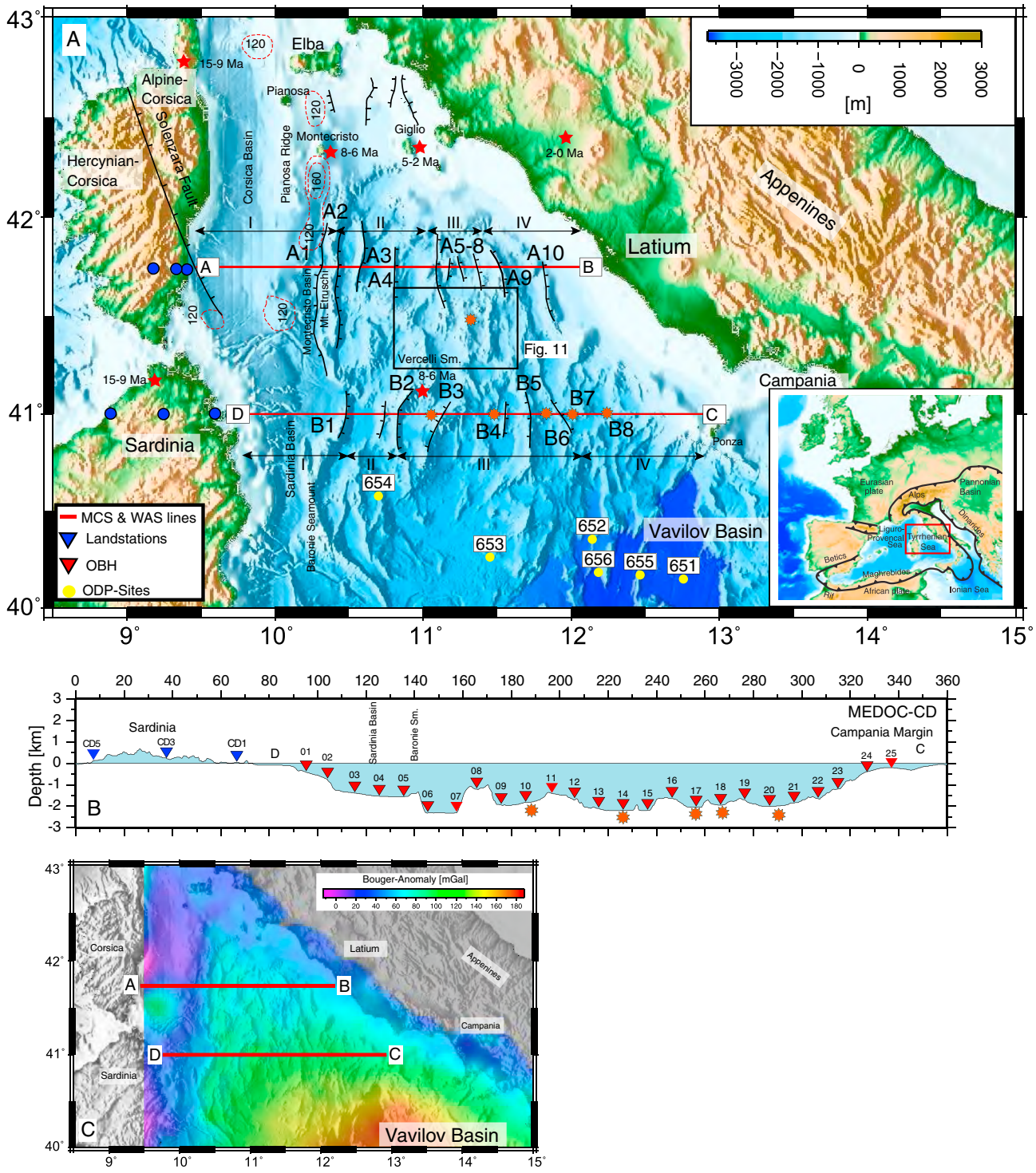

Figure 1. (a) Bathymetry map of the northern Tyrrhenian Sea [*Medimap*, 2008]. The inset (lower right corner) shows the location of the working area in the western Mediterranean and the recent large-scale plate boundary situation. Plate boundaries are taken from *Schellart* [2010] and *Jolivet et al.* [1999]. The N-S striking block structures visible in map view are labeled with A along the seismic transect AB and with "B" along the transect CD. Furthermore, lines are subdivided in zones with respect to bathymetric characteristics and velocity distribution on crustal scale wide-angle models (see Figure 3). Red stars mark locations and ages of selected magmatic samples adopted from *Savelli* [2002]. Orange asterisks mark locations where volcanic features are recognized on seismic sections presented in this study or on the bathymetry. An enlargement of the black frame is shown in Figure 13. Drill sites of the ODP Leg 107 are marked with yellow dots [*Kastens et al.*, 1988]. (b): Cross section of line CD shows the seafloor relief and the locations of the deployed ocean bottom hydrophones. (c): Gravity anomaly map shows increasing values toward the central Tyrrhenian Basin (courtesy of Getach, UK).

even recent on mainland Italy [*Savelli*, 2002, Figure 1]. The rifting phases are marked by the presence of prominent unconformities in the sediment sequence [*Trincardi and Zitellini*, 1987; *Zitellini et al*., 1986].

The work is focused on the northern sector of the Tyrrhenian Basin (Figure 1) between Corsica and the Latium Margin (Transect 1, line AB) and between Sardinia and the Campania Margin (Transect 2, line CD). Seafloor relief is smooth near Corsica (Corsica Basin) and around the Tuscany Archipelago south of Elba Island. Water depth is $<$1000 m. To the south, the seafloor is generally deeper (around 2000 m) and clearly more rugged. It is characterized by roughly N-S striking continental blocks, separated by half grabens partially filled with sediment. Most of these ridges end north of latitude ~40.5°N, where the regional water depth abruptly increases toward the south to $>$3000 m (Figure 1). This deeper water sector is the so-called Vavilov Basin with basement locally formed by basalts and serpentinized mantle rocks [*Kastens et al*., 1988; *Prada et al*., 2014].

2.1. Sedimentary Units and Unconformities

The main seismostratigraphic units of the Tyrrhenian Basin were established in 1970s as the result of several multichannel seismic (MCS) campaigns. The data were initially calibrated by sampling of seafloor outcrops [*Colantoni et al*., 1981] and later by ODP drilling in the mid-1980s (Leg 107 [*Kastens et al*., 1988]). The sedimentary package has been subdivided, from top to bottom, in three major depositional sequences: the postrift, the synrift, and the prerift sequence. They are separated by two regional unconformities: The "X" unconformity between the postrift and the syntectonic sediments and the "L" unconformity between the syntectonic and the pre-tectonic deposits [*Trincardi and Zitellini*, 1987]. Following the nomenclature adopted by previous workers [e.g., *Selli and Fabbri*, 1971], we interpret the postrift and the youngest synrift deposits as unit "A" of mainly early Pliocene to Quaternary in age, underlain by a sedimentary unit B that ranges from upper Tortonian to early Pliocene in age (ODP 654 [*Kastens et al*., 1987]). The synrift sequence is bounded at its base by the L unconformity. Where evaporites are present, e.g., at the southern and middle Sardinia Margin, earlier synrift deposits are subdivided as subunits B1, B2, and B3 with respect to post-evaporitic, evaporitic, and pre-evaporitic sequences [*Hsü et al*., 1977; *Curzi et al*., 1980]. In our study, areas B1, B2, and B3 have been interpreted here as syntectonic sequences. However, subunits of B3 have also been interpreted as prerift sediments of Tortonian to Serravallian age based on coring, e.g., at a flank of a tilted block on the Sardinia Margin [*Sartori et al*., 2001]. Within unit B, a high-amplitude reflection "Y" typically marks the top of Messinian main evaporites of unit B2 or the main Messinian erosional unconformity. It is recognizable over most of the Tyrrhenian Basin due to a strong acoustic impedance contrast across the reflector. The base of the sedimentary package is the "Z" unconformity, which may locally bounds at the top of a weak reflective seismostratigraphic unit C interpreted to be made of crystalline metamorphic rocks. However, Z is often not visible, because the reflection signature of prerift strata is rather weak. In our data, we observe an intrabasement discontinuous package of reflections mainly identified on line CD. The nature of the intrabasement unit is unclear; it could represent a prerift structure or volcanic layering with high velocities. Keeping with previous work, we label it Z throughout this contribution.

3. Data Acquisition and Analysis

3.1. Acquisition

MCS and WAS data were acquired in April and May 2010 onboard Spanish research vessel R/V *Sarmiento de Gamboa* and Italian R/V *Urania* during the Mediterràneo Occidental (MEDOC) seismic campaign. R/V *Urania* deployed 22 and 25 ocean bottom hydrophones (OBH) along lines AB and CD, respectively, with 8–10 km spacing. The profiles were extended to the west with three land stations onshore Corsica and Sardinia (Figure 1). Shooting for the wide-angle experiment was carried out by R/V *Sarmiento de Gamboa* using an array with two subarrays of 12 GII airguns with a total volume of 4600 in^3. The arrays were towed at a depth of 15 m. Subsequently, the R/V *Sarmiento de Gamboa* acquired coincident MCS lines using a 3450 m long solid state digital streamer with 276 channels with a 12.5 m channel interval and a 3040 in^3 source towed at 5 m depth. The shot interval was every 50 m, and the depth of the streamer was 10 m. This yields a common midpoint (CMP) fold of 35.

Both profiles were placed in W-E direction to study the impact of stretching on the crustal structure. The dominant fabric strikes in N-S direction, suggesting that stretching was orientated in E-W direction. This is supported by plate reconstructions [e.g., *Rosenbaum et al*., 2002]. The seafloor fabric indicates little evidence

for oblique NW-SE orientated shearing as it has been previously inferred before the basin has been mapped in high resolution. However, both domains might be separated by a transfer zone near 41°25′N.

3.2. Data Analysis and Processing

3.2.1. Refraction and Wide-Angle Reflection Seismic Data

WAS data were recorded offshore on 25 ocean bottom hydrophones. The OBH data loggers were synchronized with GPS time before and after deployment to correct for internal clock drift. The sampling rate of the loggers was 200 and 250 Hz, depending on the type of recording unit. Data were recorded in a continuous trace. Subsequently, the data were cut into single-receiver traces and converted into SEG-Y format. In the first step, the arrival of the water wave has been used to relocate the OBH position on the seafloor. Afterward, a predictive deconvolution and a time- and offset-variant Butterworth filter were applied to improve the signal-to-noise ratio. For the deconvolution, we used a prediction lag of 0.23 s and an operator length of 1 s to suppress reverberations related to the oscillating signal of the airgun. On line CD, three stations (OBH04, OBH07, and OBH11) failed to record useful data. The remaining 22 OBH stations have good data quality and excellent quality on the land stations onshore Sardinia. Examples of land station (CD3, vertical component) and OBH stations (OBH05 and OBH12) are presented in Figure 2. All land stations recorded Pg phases between offsets of 40–120 km and excellent Pn arrivals travelling through the upper mantle up to the maximum offset of 300 km. A wide-angle arrival at 3 s and 40–80 km offset was first assumed to be the Moho reflection underneath Sardinia, but during modelling, it became clear that it was difficult to model this arrival as a PmP. It arrived too early for a reflection coming from the crust-mantle boundary, and it might rather be related to an intracrustal reflection or to a side echo reflection.Later, weaker reflected arrival between 60 and 80 km offset at 4–4.5 s fits better as *PmP* reflection. The records of OBH05, located in the Sardinia Basin, show first arrivals of Pg phases that are clearly identifiable to a maximum offset of 40–50 km. Reflections at 4.5–5 s and 30–60 km offsets could be identified as *PmP* reflections. At offsets larger than 60 km, the identification of the first-arrival onset is more difficult. A clear correlation is not possible. Also at station OBH12 (center of the profile), Pg arrivals are clearly identified to 50 km offset and *PmP* reflections up to 70 km offset. Larger offsets were not used due to a decrease of the S/N ratio. Pn phases were not reliably identified on OBH records. The accuracy of arrival time picking increases from 50 ms at near offsets to 100 ms at far offsets for refracted arrivals and *PmP* reflections. These picking uncertainties also include phase changes and time shifts related to filtering and the applied statistical deconvolution.

After phase identification and travel time picking, the data were first modeled with the forward modeling code Rayinvr [*Zelt and Smith*, 1992]. This forward approach was aimed to achieve a reasonable initial velocity field. The land and seafloor topography for the model input was gridded at a spacing of 750 m. The data came from a global topography grid [*Smith and Sandwell*, 1997] and from multibeam echo sounder data collected during the survey. The results of the MCS data were used to define the geometry and interval velocities of the sediment-filled grabens along the profile. The graben geometry and infill velocity are well constrained from focusing analysis and iterative prestack depth migration. The forward velocity model was used as initial model for a tomographic travel time inversion with tomo2D [*Korenaga et al*., 2000] that jointly inverts for arrival times of both refracted and reflected phases. The cell size of the velocity field was 200 m in horizontal direction and 100 m in the vertical direction, increasing to a cell size of ~500 m at a depth of 30 km scaled by a square root function. We first inverted for Pg arrivals recorded at the near offset range (0–15 km) showing an apparent higher-velocity gradient in the upper part of the crust and subsequently for all Pg phases up to 50 km offset (Table 1). Afterward, Pg phases were jointly inverted with the *PmP* reflections. After eight iterations, the RMS misfit for the crustal model converged to 87 ms. Finally, we included the travel times of Pn and overdamped the velocity variations above the crust-mantle boundary by a value of 200 [*Korenaga et al*., 2000]. The final velocity model including the Pn phase has a misfit of 94 ms (Figure 3). For the parameterization of the tomographic inversion, we tested various combinations of vertical and horizontal correlation lengths for velocity nodes as well as smoothing and damping parameters. For the final models, we used a horizontal correlation length of 1 km at the top of the model increasing to 5 km at the bottom. Vertical correlation lengths were set to 0.75 km and 2 km, accordingly. Smoothing values for velocities and depth were set to 170 and 40 and 30 and 20 for the damping [*Korenaga*, 2000]. The correlation length for the Moho reflector was 5 km. The inversion was equally balanced for velocity and depth nodes.

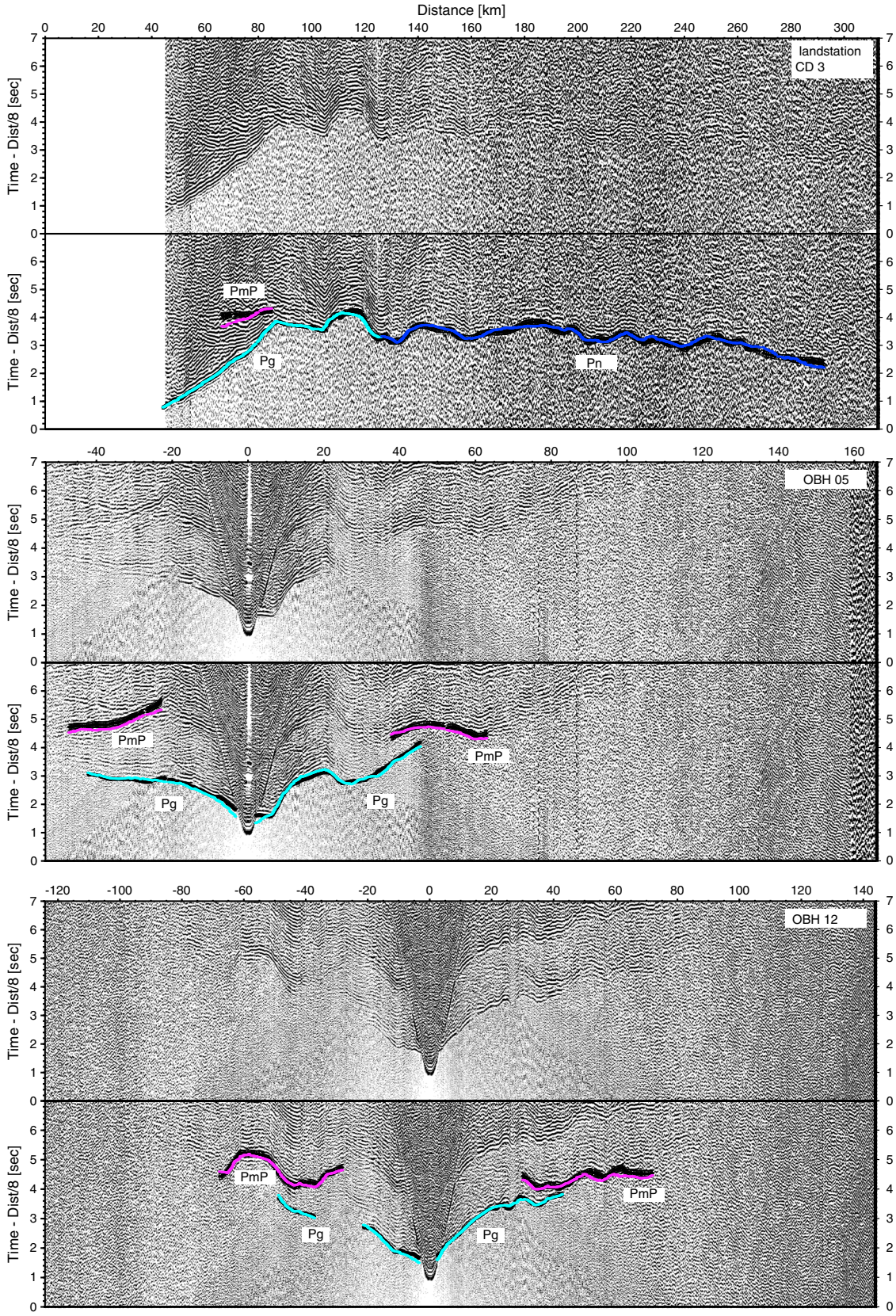

Figure 2. Three examples of record sections of the Line CD. For locations, see cross section in Figure 1. Travel time picks including pick uncertainties are used for forward modelling and subsequent tomographic inversion. Travel times obtained from the inverted model are light blue (Pg), blue (Pn), and pink (*PmP*).

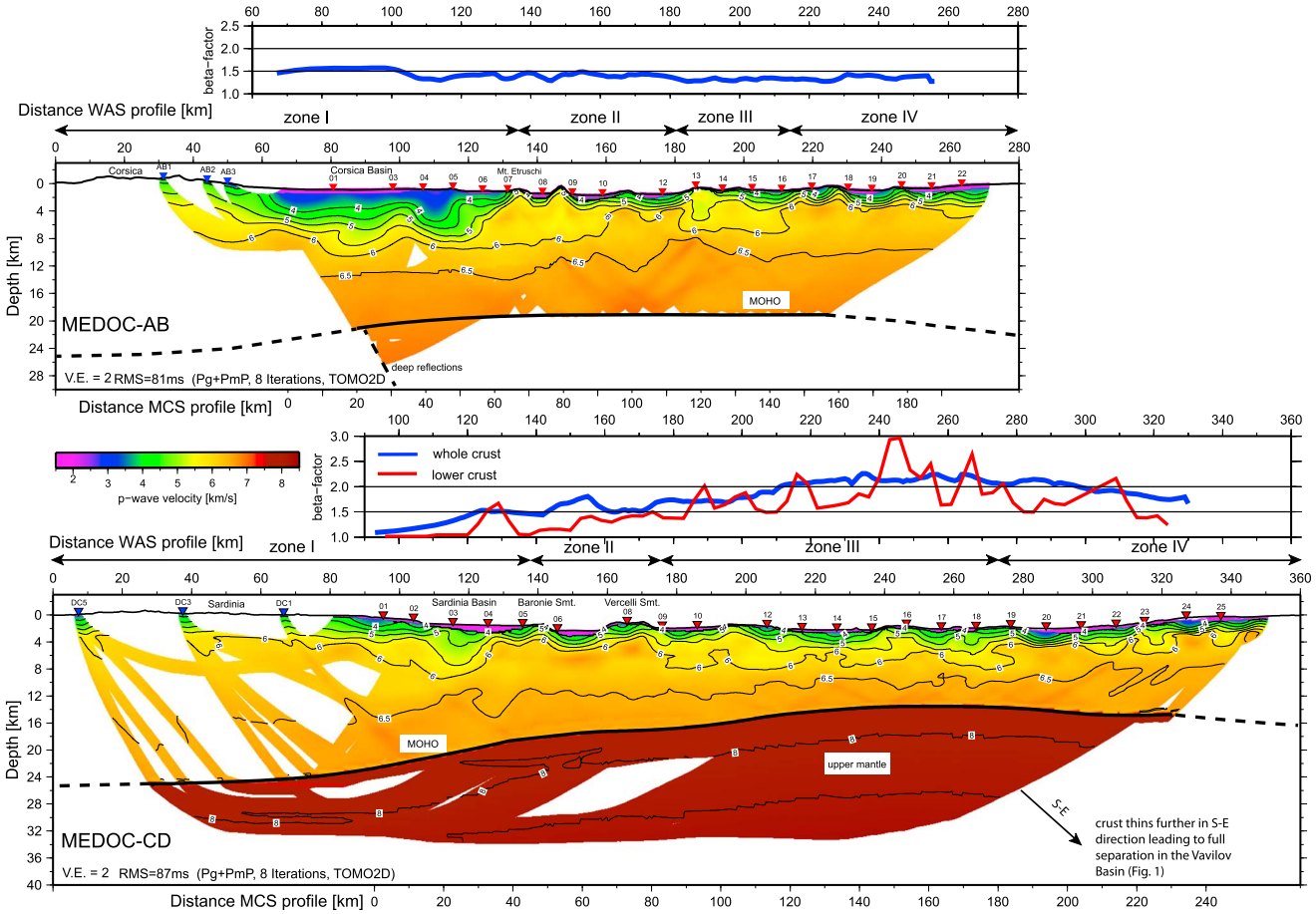

Figure 3. Results of the travel time inversion using the code tomo2D [*Korenaga et al.*, 2000]. The two transects are divided into four zones (I–IV) dependent on a prominent topographic feature (zone I) and differences in velocity distribution (zones II–IV). By identifying the top of the crystalline basement (in PSTM data), we estimated the crustal thickness and calculated the β factor along the profiles assuming an initial thickness of ~24 km (blue line). For line CD, we calculated also the stretching factor for the lower crust by the thickness between the 6.5 km/s isoline and the Moho.

3.2.2. Model Uncertainties

To check the robustness and uncertainties of the final model, we generated a set of modified starting models. The modifications were: (1) Increasing or decreasing the crustal velocities by 5%, except for the velocities in the upper sedimentary cover, which are well defined with the MCS data. (2) Variations of crustal thickness by ±1, 2, and 3 km. (3) A combination of the ±3 km change of thickness with the ±5% velocity perturbation. Additionally, we included some previous models that were developed during the stage of parameter testing. With this set of 18 models, we calculated an average velocity field and the standard deviation [*Korenaga et al.*, 2000] that yields the uncertainty of the model (Figure 4a). The results show that the upper crust modeled velocities have $<$0.1 km/s uncertainty. Here ray density is high as indicated by the derivate weight sum (Figure 4b). Between 180 km and 280 km, velocity uncertainties are small across the entire crust. This area is well constrained by Pg phases travelling 12–16 km deep into the model. Across the model, velocities in the middle and lower crust have uncertainties of ≤0.2 km/s. The higher uncertainty of 0.3 km/s in the upper crust at 160 km is explained by the failure of OBH07 and the absence of crossing rays constraining this area. At the eastern part of the profile, stations recorded fewer arrivals travelling through the middle crust. Here velocities in the lower crust are mainly determined by *PmP* reflections, yielding higher uncertainties (~0.2 km/s). Velocities in the upper crust under Sardinia and Sardinia Margin show uncertainties of 0.1–0.15 km/s in spite of no reversal shooting across the onshore domain. Pg phases observed at OBH01–OBH06 cross the Pg phases of the land stations and may mitigate velocity uncertainties under Sardinia.

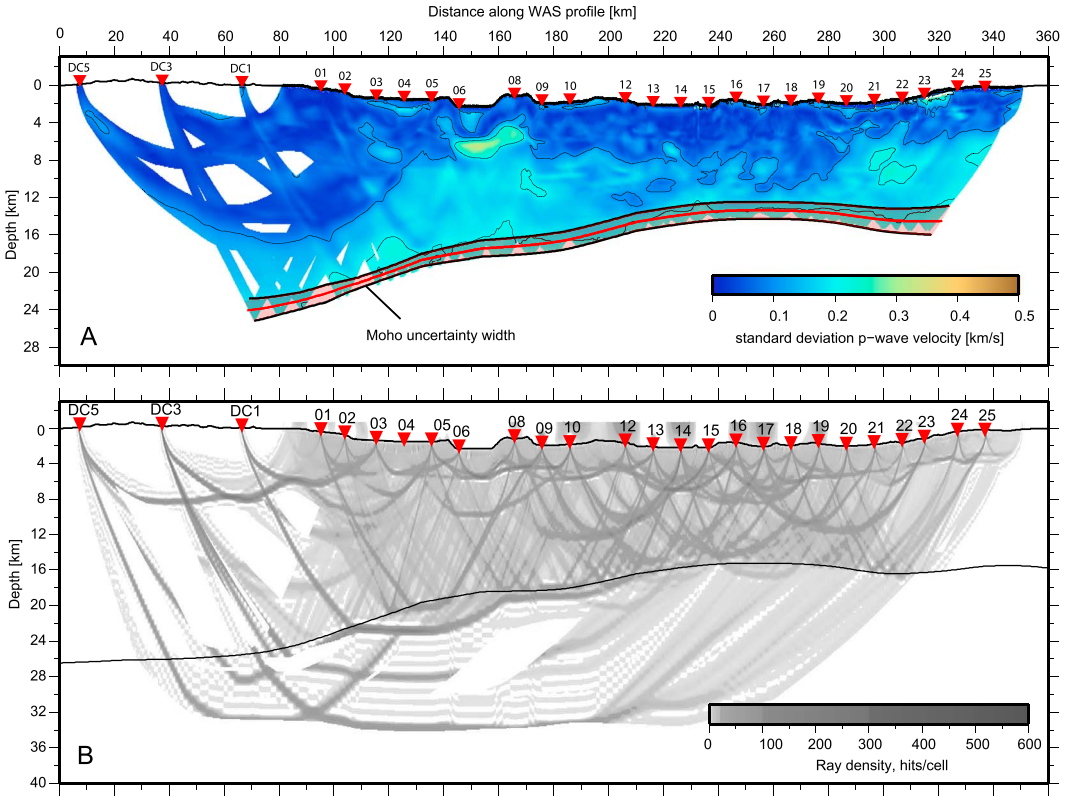

Figure 4. Uncertainties of *P* wave velocities along the line CD. The uncertainties are estimated by calculating the standard deviation by a set of perturbed starting models. Moho uncertainties are in the range of ±2 km beneath Sardinia and the Campania Margin and ±1 km in the center of the profile.

The uncertainty in Moho depth is ±2 km underneath Sardinia, Sardinia Margin, and Campania Margin. Between 180 km and 280 km, the uncertainty of Moho depth is ±1 km due to high ray density. No Pn phases were identified at OBH stations, and no rays traveling through the uppermost mantle cross the Pn rays recorded by the land stations. Thus, velocity uncertainties in the mantle could not be statistically determined. However, as we damped the upper crust during the inversion including the Pn phases, we forced modifications of the velocity field to be mainly limited to the mantle.

3.2.3. Multichannel Seismic Data

The software packages OMEGA2 (WesternGeco) and SIRIUS (GX-Technology) were used for MCS seismic data processing and prestack time migration. In the first step, we set geometry, applied a bandpass filter to the data, and suppressed the reverberations of the air gun signal by applying a statistical deconvolution to the shot gathers within a design window below the seafloor reflection. Surface-related multiples were attenuated by the prediction of the propagating wavefield. The method was fully data driven and did not require any information about the water bottom topography [*Verschuur et al*., 1988]. The predicted surface-related multiple model was subsequently adaptively subtracted from the original data.

Afterward, the data were sorted into CMP gathers, and focusing analysis and iterative prestack depth migration were carried in order to build a first velocity field for the reflective sedimentary and upper crustal parts. After that, the velocity was modified in a way that primary reflections dip upward and multiples downward. Subsequently, f-k filtering was applied to further attenuate the remaining multiple energy. An inside mute was additionally applied to remove the multiples at near offsets. An outside mute removed the refracted arrivals at far offsets. Focusing analysis with SIRIUS was carried out for the second time to build a final velocity model. In the weak/nonreflective crystalline crust, velocities were adopted from inversion result of WAS data. The final velocity field was transformed into two-way travel time and used for partial stacking (stack width of 200 m) and subsequent PSTM. The final results of both sections are presented in Figure 5. We transformed the velocity field obtained by the WAS data into two-way travel time (TWTT) and overlaid on the time-migrated sections.

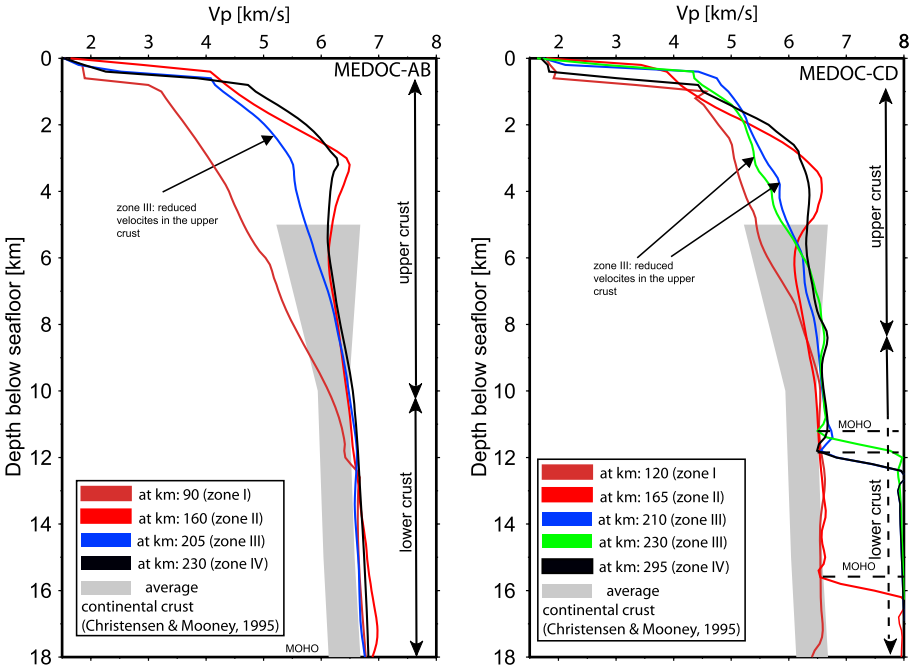

Figure 5. 1-D velocity-depth profiles extracted from line AB and line CD. Note that within zone III, the velocities in the upper crust are lower than in the surrounding areas. Velocities at depth of 5–12 km match the global average velocities in continental crust [*Christensen and Mooney*, 1995] and are insignificantly higher in the lower crust.

4. Results

Tomographic inversion of WAS data and PSTM images provided complementary information for the geological interpretation. Based on the continuity of tectonic structures like Mount Baronie (B1) and Mount Etruschi (A2), well displayed in bathymetry in Figure 1, and on the along-strike variations in the wide-angle velocity models (Figure 3), we have divided both seismic lines into four zones (I–IV) with distinct characteristics (Figure 3). Zone I is composed of the islands of Corsica and Sardinia and the Corsica and Sardinia Basins bounded to the east by blocks B1 and A2. Zone II consists of large, rotated block structures with higher-velocity gradient than adjacent zone III, where a significantly lower velocity gradient is observed. This can be seen on 1-D profiles extracted at different locations (Figure 5) as well as in the velocity models (Figure 3). Zone IV includes the Latium and Campania Margins approaching the mainland of Italy, where the velocity gradient comparatively increases. We differentiate an upper crust (UC) characterized by $Vp < \sim 6.0–6.3$ km/s, typical of continental upper crustal rocks [*Christensen and Mooney*, 1995], and a lower crust (LC) with $Vp > 6.5$ km/s. We use these definitions to estimate stretching factors for the whole crust and for the lower crust (Figure 3). Velocity models from unthinned crust or thickened crust derived from earthquakes or previous wide-angle experiments around Italy fall also within this range of the average velocity of continental crust [e.g., *De Luca et al*., 2004]. For unstretched prerift crustal thickness, we assumed the thickness of Corsica and Sardinia islands of ~24 km [*Contrucci et al*., 2005; *Mele and Sandvol*, 2003]. At the Tuscany Margin, modeling from wide-angle data showed a comparable thickness of ~25 km [*de Franco et al*., 2000]. For the LC, we assumed an initial thickness of 7 km as observed beneath Sardinia and the Sardinia Margin. Stretching factors were calculated where MCS data are available (Figure 3). The description of line AB is briefly presented. A detailed description of the prestack depth-migrated section is presented elsewhere [*Moeller et al*., 2013].

4.1. Zone I: The Corsica and Sardinia Margin

This zone contains the 50 km wide Corsica and Montecristo Basins imaged on line AB and the 30 km wide Sardinia Basin imaged on line CD (Figure 1). The Corsica Basin hosts a thick pile of sediment imaged to 4.5 s TWTT (Figure 6). The basement below the Corsica Basin has velocities increasing from ~5 km/s to ~6 km/s to a depth of ~6 km (Figures 3 and 6). Unit A is a posttectonic sequence, well stratified, and

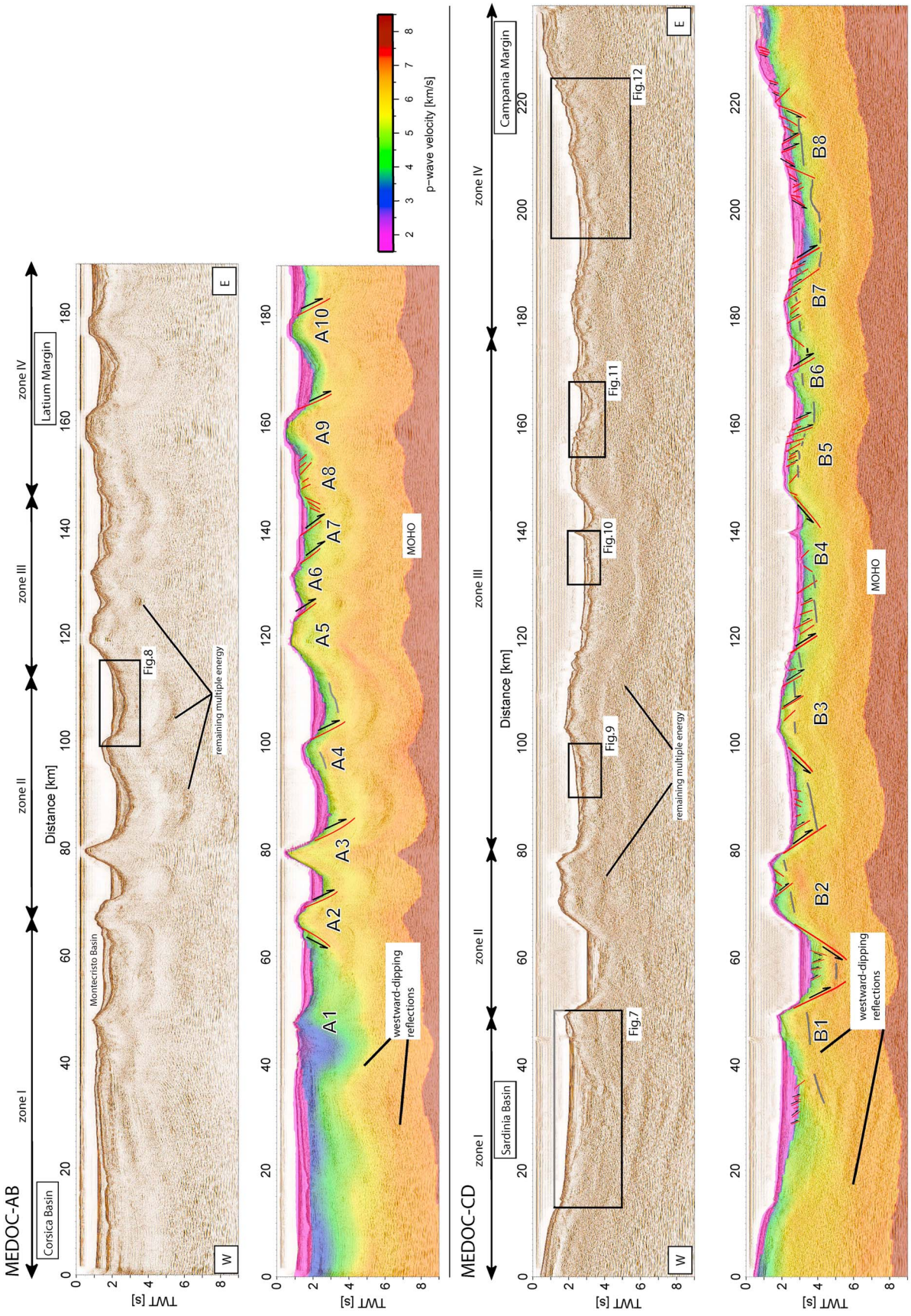

Figure 6. Results of the prestack time-migrated sections with and without overlay of the velocities obtained by the inversion of wide-angle data. The main block-bounding faults are drawn on top. Line AB presents the Corsica Basin and the horst and graben structure toward the Latium Margin. Flat block summits near the Latium Margin indicate that this part was emerged above sea level, when rifting commenced. At the Sardinia Margin (line CD), two large blocks bound the deepest subbasin in this profile whereas the block size diminishes eastward and the numbers of faults increase. A common feature observed on both lines are internal westward dipping reflections bounding the Corsica and the Sardinia Basin to the east. Reflections of the Moho cannot clearly be observed on the PSTM sections as their travel times are expected to occur at the same TWTT than the remains of the multiple. The gray line drawings mark the appearance of an almost continuous intracrustal reflector (*Z*) which is offset by fault-bounded blocks. The Z is perhaps related to the top of a thin volcanic sheet with higher velocities.

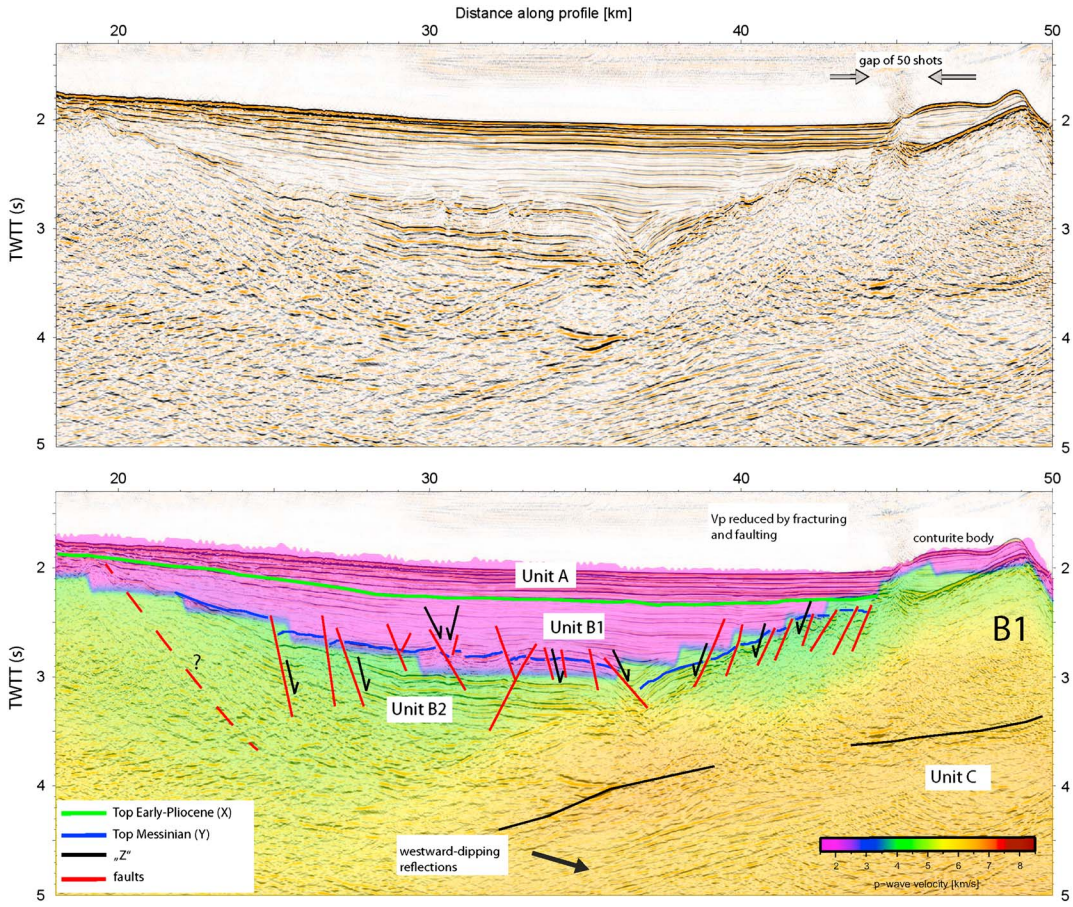

Figure 7. Enlargement of the Sardinia Basin. See Figure 6 for location. The basin contains a 0.3 s TWTT thick layer of posttectonic deposits (unit A) followed by the post-evaporitic and Messinian high-amplitude reflectors (*Y*). The upper part consists of thin and fine layers whereas the lower part consists of thick reflectors. Syntectonic and posttectonic reflections are onlapping on tilted block B1. Internal reflections within this block indicate rotation direction.

horizontally deposited (Figure 6). Detailed seismic images are provided by *Moeller et al.* [2013]. A clear boundary with unit B1 is not observed. B1 thins from 0.6 s to 0.15 s from west to east. The Y unconformity at the top of unit B2 can be traced through the entire Corsica Basin as an erosional unconformity cut by canyons. Underneath the Messinian deposits, the older Miocene infill is fan shaped. This feature can be interpreted as a syntectonic sequence, deposited during the formation of the Corsica Basin that probably started ~30 Ma ago in the Oligocene [*Mauffret et al.*, 1999]. The sedimentary sequence terminates against a series of westward dipping reflections near the Pianosa Ridge, where reduced *P* wave velocities occur near the surface (Figure 6). We interpret this feature as caused by fracturing in the upper 2–3 km of a tilted continental block rotated on the fault that bounds Corsica Basin to the west. The feature might have been also interpreted as related to thrusts of a former collisional prism [*Mauffret et al.*, 1999]. In the adjacent Montecristo Basin, a sequence of postrift, synrift, and prerift strata is observed. Synrift strata are Messinian in age, indicating that this subbasin developed after the formation of the Corsica Basin [*Moeller et al.*, 2013]. Moho reflections (*PmP*) underneath the Corsica Basin constrain that the crystalline crust is 15 ± 2 km thick, similar to the measurements farther north [*Contrucci et al.*, 2005], implying a β factor of ~1.5 (Figure 3).

Farther south, the infill of the Sardinia Basin consists of a 0.3 s TWTT thick unit A, thinner than the ~0.5 s TWTT in Corsica Basin. The unit seems to be undisturbed and underwent little tectonic activity (Figure 7). Below unit A, the X unconformity bounds the top of unit B, which is ~1.6 s thick. This sequence of early Pliocene to Messinian age can be clearly divided into an upper and a lower sequence [*Curzi et al.*, 1980], which is cut by small offset normal faults. Its base is bounded by the high-amplitude Y reflector which has been related to evaporites of Messinian age along the Sardinia Margin [*Fabbri and Curzi*, 1979], but no evidence of evaporite

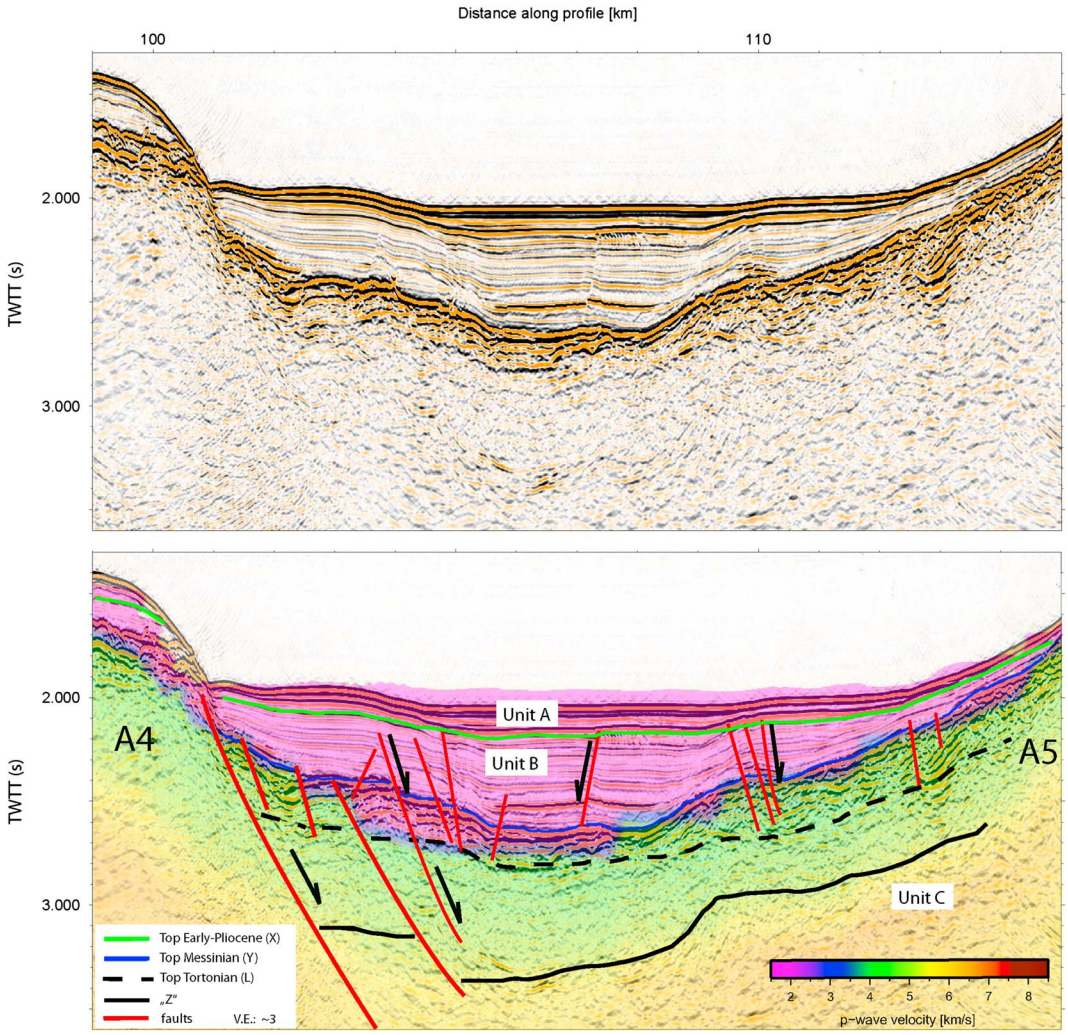

Figure 8. Example of the stratigraphic units in the northern line AB in zone II between blocks A4 and A5. Horizontally layered deposits (unit A) are post-tectonic. Below, the early Pliocene and Messinian (syntectonic unit B) and the basement (unit C) are cut by normal faults. The weak reflector Z might be the basement of the prerift crust or an internal (maybe folded) layer within the crystalline basement. It coincides with a change in velocity from 4.5 to 5.5 km/s. For location, see Figure 6.

deposits is observed in our images. A pre-evaporitic subunit B3, as it has been observed at the Sardinia Margin farther to the south [*Curzi et al.*, 1980], is not observed in the entire investigation area. At the Y reflector unconformity, *Vp* changes from 2.0 km/s to ~3.5–4.0 km/s related to a change in strata character. Due to the deposition during the active rifting, the entire sequence is fan shaped and tilted. Where the Messinian sequence terminates against the tilted block B1, the velocities increase suddenly to 5.5 km/s in the lower part and to 4.5 km/s in the upper part of the block. The reduced velocities coincide with an area of intense faulting (Figure 7), indicating a relationship between both observations supporting a structural correlation of the two data sets. The PSTM images show that internal reflections of block structures can be identified to ~7 s TWTT dipping toward the west (Figures 6 and 8). We interpret that the top of the intrabasement dipping reflections is horizon Z, which is seen on other rotated blocks farther east (Figure 6). The dip direction is similar to those reflections that bound the Corsica Basin to the east (A1), which appears to support that at least some of those reflections may be related to tilted prerift strata.

In zone I, the *Vp* of the UC (Figure 5) falls within velocities typical for continental crust [*Christensen and Mooney*, 1995]. In the lowermost crust, however, the *Vp* of 6.5–6.7 km/s are slightly higher than the average continental crust (Figure 5). The crust underneath Sardinia is 24–25 km ± 2 km thick and along line CD has been thinned by a factor of ~1.3–1.5 to 16–19 km at the Sardinia Margin (Figure 3). This is slightly thicker than the crystalline crust underneath the Corsica Basin.

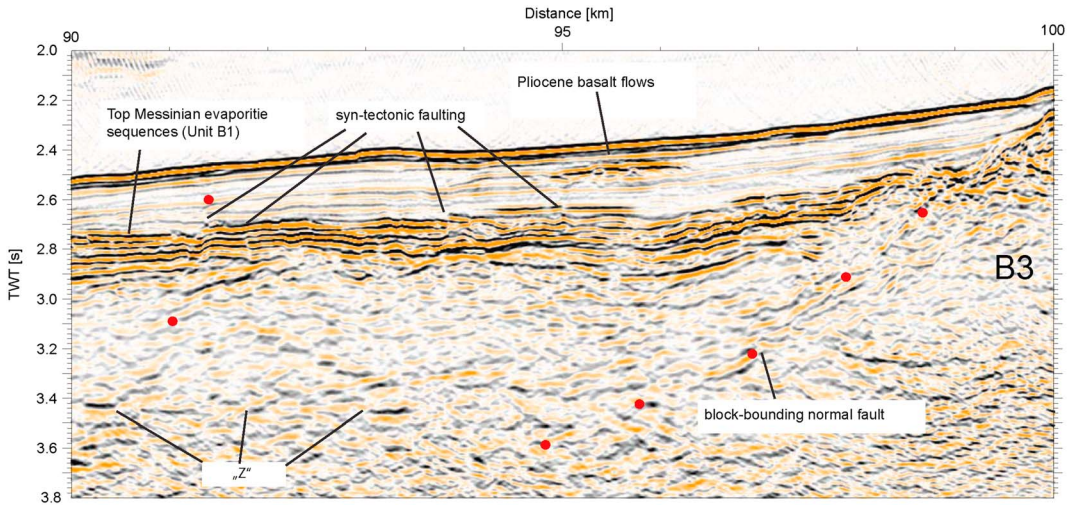

Figure 9. Close up of the PSTM section from zone III. Below the posttectonic sequence, fine laminated, party discontinuous, reflections might belong to layers of gypsum of Messinian age interbedded with sediments [see Site 654 ODP Leg 107, *Kastens et al.*, 1987, 1988]. Faults cut through this layer and indicate high fracturing. For location, see inset in Figure 6.

4.2. Zone II: Deep Subbasins

East of the Corsica and Sardinia Basin, the basin is characterized by large horst and graben structures (Figure 1). Zone II is characterized by the greatest water depth and the deepest top of basement; basins are bounded by rotated fault blocks A2 and A5 and B1 and B2 (Figure 6). The grabens bounded by blocks A4 and A5 contain a subhorizontal, ~0.2 s TWTT thick unit A. Normal faults indicate active extension during the deposit of unit B during Pliocene and Messinian time (Figure 8). The top Messinian is marked by a high-amplitude reflection Y bounding partly chaotic internal structures. Across the Y horizon, *Vp* increases rapidly from 2 km/s to 3.5–4 km/s. Under the Messinian sequence, there exist potentially prerift strata imaged as weak reflections, bounded at the top by a discontinuous reflection interpreted as the Z horizon, that marks a velocity increase from 4.5 to 5.5 km/s. In this zone, the geometry of the Moho is subhorizontal and the crustal thickness of 17 ± 1 km yielding ~30% stretching (Figure 3). The graben east of the Sardinia Basin is bounded by the large B1 and B2 fault blocks, forming the deepest structure along the line CD, where the seafloor of the western flank deepens from 1000 m to 2300 m water depth (Figure 6). The sediment infill of the graben shows a sedimentary sequence similar to the infill of the Sardinia Basin (Figure 8). Small chaotic features in the sediment sequence are likely to be related to debris flow deposits from the steep flanks. The lower Messinian is a fan-shaped geometry. Reflections within the upper part of block B2 dip west and follow the velocity isoline of ~5.5 km/s of the wide-angle seismic model (Figure 6). The wide-angle velocity model shows a velocity increase from 4 km/s at the top of the block to 6 km/s at ~3 km depth and to 5 km/s at ~12 km depth (Figure 5). The lower crust is ~5 km thick with velocities of 6.5–6.7 km/s. The crust in zone II has thinned by a β factor of ~1.7 and is 3 4 km thinner than on the line AB.

4.3. Zone III: Highly Fractured and Thinned Crust

The WAS velocity model of line AB reveals a 40 km wide zone (Figure 3), where the velocity gradient of ~0.5 s^{-1} to a depth of 4–5 km is lower than the ~1 s^{-1} of the surrounding zones II and IV (Figure 5). In zone III, the fault block size (A5–A8) decreases, in comparison with zones II and IV, while the number of faults increases, e.g., the fractured block A8. However, there are no substantial variations of the ~17 km crustal thickness along line AB compared to the decrease to ~11 km on line CD. Zone III on line CD is characterized by a similarly abrupt decrease of velocities in the upper crust, similar to zone III on line AB. The 1-D velocity-depth profiles in Figure 5 show that the ~0.3 s^{-1} gradient of the upper crust is reduced to 5–6 km depth below seafloor, compared to velocities at zone IV with a ~1 s^{-1} gradient. This comparative reduction in velocity is of ~12%. The PSTM of line CD in zone III images similarly fault block size reduction (Figure 6) and faulting increases. However, faults in zone III do not generate large horizontal displacements like for the blocks B1 and B2 in zones I and II (Figures 9, 10, and 11). The minimum penetration of faults in zone III is

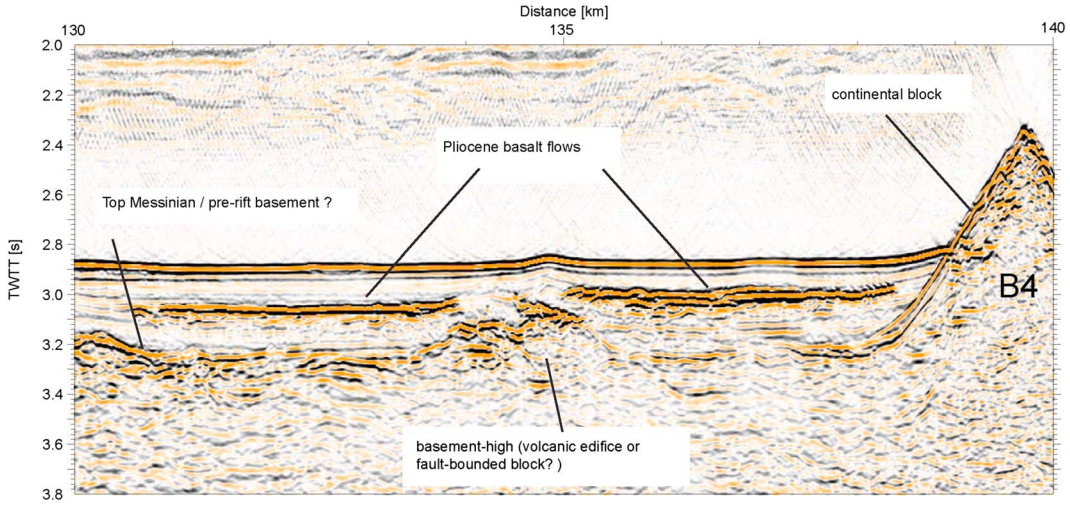

Figure 10. High-amplitude reflections in zone III located within the posttectonic sediments (Pliocene) are likely to be basalt flows (e.g., drilled at Site 654, ODP Leg 107). The basement high may correspond to a volcanic edifice. The top of the basement below the basalt flows might represent Messinian deposits but could also be prerift layers or older volcanic flows. For location, see inset in Figure 6.

indicated by offsets of intrabasement horizon Z (Figure 11). Where Z is absent or weak, faults are just recognized within sedimentary deposits and top basement offsets. However, it seems reasonable to suggest that WAS velocities of ~6 km/s at 5–6 km depth may represent fractured and/or altered upper crustal rocks (Figure 3). Deeper in the basement, *Vp* increases rapidly from ~6 km/s to 6.5 km/s within 2–3 km at midcrustal levels. The lower crust is 3–4 km thick with *Vp* of 6.5–6.6 km/s. Zone III is also a region where the crust has been thinned most to ~11 km thickness corresponding to a stretching factor of ~2.2 (Figure 3). Crustal thinning is similar to the long-wavelength thinning trend estimated for the lower crust by a factor ~2. Moho reflections on the MCS data are poorly imaged, because remains of the multiple occur at the same TWTT and unfortunately primary are not discernible from multiple remains.

The sedimentary unit A has a 0.2–0.3 s TWTT thickness and locally 0.4 s in the deeper grabens. On top of the main blocks, unit A is disturbed by high-angle faults reaching the seafloor (Figure 11), but its deposits are undisturbed in some grabens. The Messinian unit is partly finely stratified (Figure 9) but in places fractured and chaotic, or even unstructured (Figure 10). The Z horizon within the basement and similar strata below are

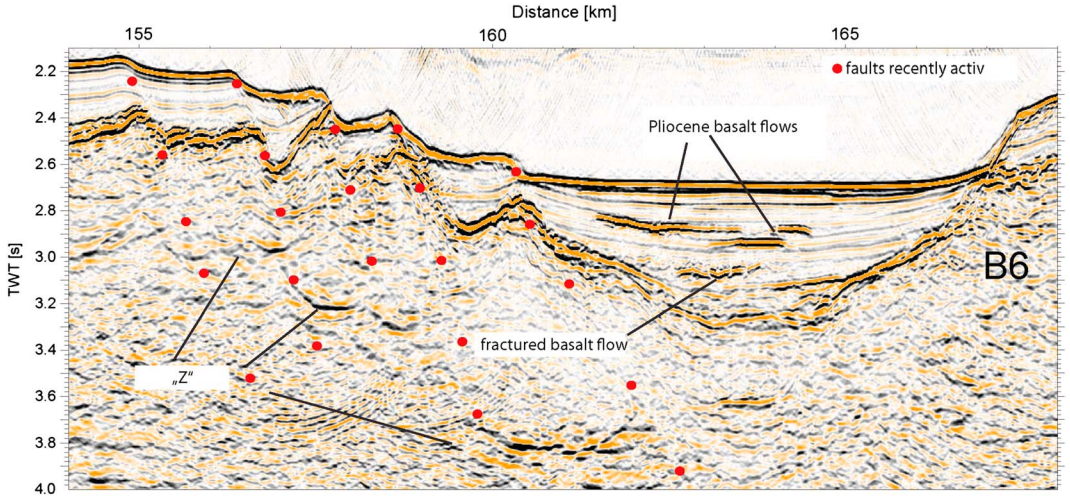

Figure 11. At least three volcanic eruptions are recorded within this subbasin in zone III. Faults cutting through block B5 crop out at the seafloor and indicate recent tectonic activity. The basement layer Z is offset by those faults and is in nature rather a lithological interface than a detachment. For location, see inset in Figure 6.

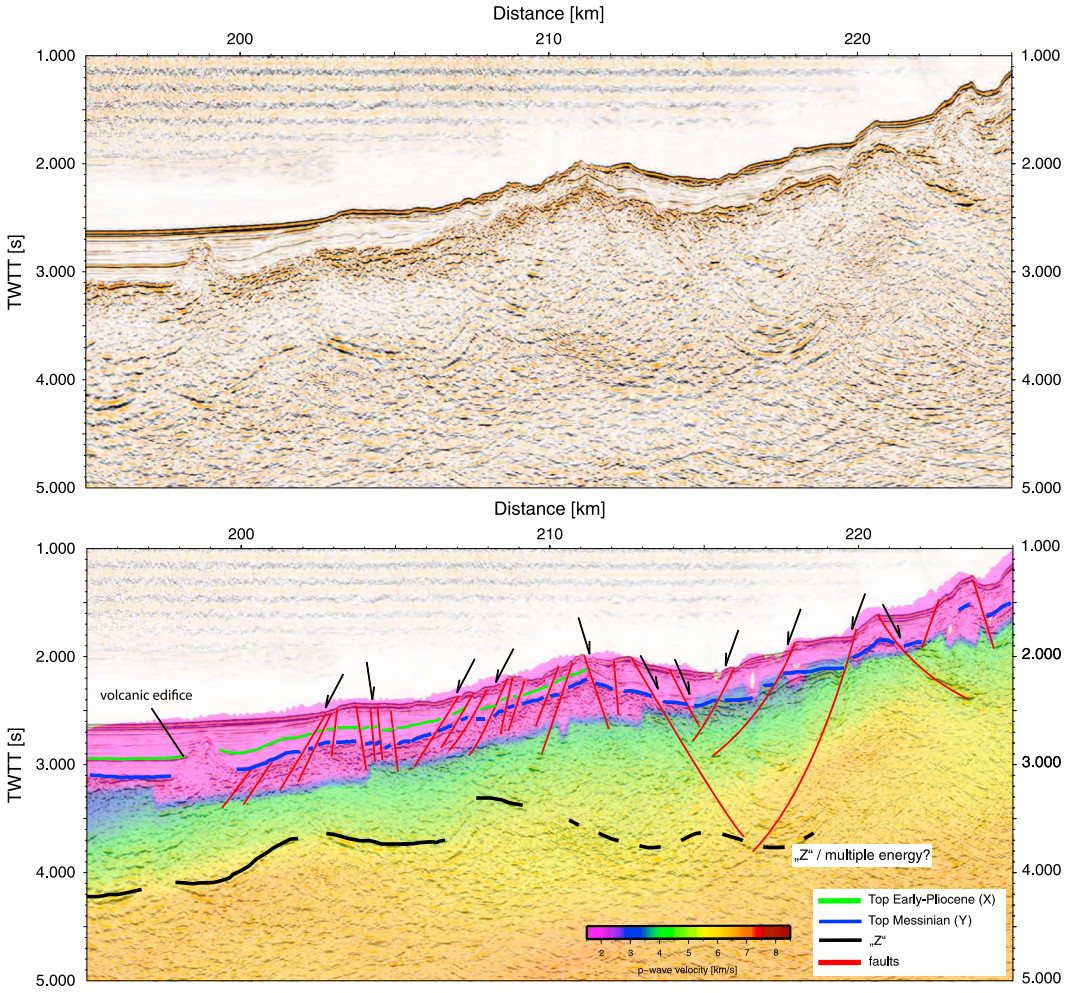

Figure 12. Zoom into the eastern part of line CD. Faults cut through the seafloor and indicate that tectonic activity has not fully ceased. A cone-like structure is assumed to belong to a volcanic feature. The internal basement reflector Z coincides with the velocity change from ~4.5 to 5.5 km/s and might represent the same reflector observed farther to the west (Figures 8 and 9).

present across zone III. They are associated to a *Vp* change from 4.5 to 5.5 km/s. Within the foot and hanging wall of faults blocks, Z is tilted and offset by faults.

The PSTM images show high-amplitude reflections within the Plio-Pleistocene sediments (Figures 9, 10, and 11). They have the polarity of the seafloor reflection and thus are not low velocity, e.g., caused by the presence of free gas. These reflections can be interpreted as magmatic sills or flows, probably similar to the basaltic layer of 2 m thickness drilled during the ODP Leg 107 at Site 654 (Figure 1) at a depth of 80 m below seafloor [*Kastens et al.*, 1988]. Due to the rapid cooling history, it was assumed that this shallow basaltic layer was an extrusive lava flow and not a sill. The widths of the magmatic layers range between 1 and 3 km on the seismic images. In the flat area between the block B3 and B4 (Figure 10), apparently two basalt layers of ~3 km extent come close to a basement high. This might be a small continental block or a volcanic edifice. In Figure 11, the basaltic extrusions between blocks B6 and B5 occur at three depth levels within the Pliocene deposits. The lowermost basaltic layer is clearly fractured.

4.4. Zone IV: The Latium and Campania Margin

Block size increases in the Latium Margin (line AB) where blocks A9 and A10 are bounded by major faults dipping east. Intense, small-scale faulting like in zone III is not observed in the PSTM images and may be related to the increase in *P* wave velocities. The flat summits of blocks A9 and A10 and angular unconformity truncating the overlying strata indicate wave erosion, suggesting that this area was above sea level during the early rifting (Figure 6).

In the Campania Margin (line CD), the crust is 13 km thick implying a β factor of ~1.8. The sedimentary unit A is cut by high-angle normal faults reaching the seafloor. The underlying Messinian unit B is comparatively thinner, predominantly discontinuous or absent. Faults intersect this unit and cut also through the underlying basement (Figure 12). At 199 km, a triangular shaped body buried by posttectonic sediments is underlain by short reflections of high amplitude with reflectivity of characteristics similar to Z. The area of these reflective patterns coincides with a velocity anomaly between 270 km and 300 km (Figure 3) reaching 6 km/s just 2 km below the seafloor (Figure 3). An undulating, east dipping continuous reflector of low frequency and high amplitude occurs within the basement between 190 km and 220 km at 3.5–4 s TWTT that may represent the Z horizon (Figure 12).

5. Discussion

Results from the PSTM and WAS data provide new information to further understand the evolution of extension in the northern Tyrrhenian Sea Basin. The PSTM sections display the sedimentary and tectonic structure. Crustal thickness and velocity distribution obtained by tomographic inversion provide constraints on the variations of crustal structure related to basin formation processes and rift evolution. Our main observations are as follows:

(1) Along line AB, the crust has thinned homogeneously by block rotation and crustal thinning with a stretching factor of 1.3–1.5 [*Moeller et al*., 2013]. Extension concentrated from upper Tortonian to early Pliocene. (2) Along line CD, the crust thinned to a stretching factor of 1.3–1.5 on the western Sardinia Margin and to a maximum of 2.2 near the Campania Margin (Figure 3). (3) On both lines, we observe a decrease of the intrabasement velocity gradient in zone III near the basin center. The change in depth velocity gradient spatially coincides with a decrease of fault spacing and an increase in the amount of comparatively smaller faults binding smaller blocks than in other zones of the profiles. (4) On line CD, the seismic image reveals an intracrustal reflection Z that is offset by normal faults and may represent a volcanic layer. Moreover, several kilometer-wide, high-amplitude reflections within the posttectonic and syntectonic sedimentary deposits have been interpreted as magmatic extrusive layers similar to that drilled at ODP Site 654 [*Kastens et al*., 1988].

5.1. Temporal and Spatial Distribution of Deformation

The timing of the main rift phase has been interpreted from the geometry of the sedimentary sequence and faults bounding the grabens. The absence of important faulting and the uniform stratification of the late Pliocene to Holocene sediments (unit A) covering line AB east of the Corsica Basin indicates that extension was not occurring during this time interval. High-angle normal faults cut the strata up to early Pliocene age, indicating the age of the end of rifting here. Underlying strata are tilted and display a fan-shaped geometry. Faulting indicates that the main rift phase occurred between upper Tortonian to Messinian age. The amount of rotation of the hanging wall and footwall blocks (A5–A7) changes with age, and it can be inferred that extension during rifting may have migrated sequentially eastward [*Moeller et al*., 2013]. Based on geological and older seismic images, it has been inferred that the opening of the basin started in late Miocene or upper Tortonian age [e.g., *Rosenbaum and Lister*, 2004; *Sartori* 1990]. It has been proposed, e.g., based on ages of volcanic rock samples [*Savelli*, 2002], that the rift migrated eastward probably related to subduction rollback [*Jolivet et al*., 1999; *Faccenna et al*., 2001; *Rosenbaum and Lister*, 2004]. However, based on the age of the syntectonic sequences of zones II–IV on line AB, the propagation is very limited. This excludes the evolution of Corsica Basin because its development is related to an earlier extensional stage that started circa 30 Ma in the Oligocene [*Mauffret et al*., 1999]. Along line CD, we observe a change in the age of deformation and thickness of the syn-sedimentary and post-sedimentary deposits from west to east that clearly support the progressive migration of the main rift deformation to the east.

At the Sardinia Margin (zone I and II), thick late Pliocene to Holocene sedimentary structures are undisturbed (posttectonic), but the underlying early Pliocene to Messinian upper and lower deposits [*Hsü et al*., 1977; *Curzi et al*., 1980] are offset by normal faults indicating syntectonic deposition (Figure 7). This relationship is similar to that of the Messinian sequences imaged on line AB and implies that this area and the Sardinia Margin evolved contemporaneously.

Within zone III of line CD, Messinian deposits are markedly thinner but still present (e.g., Figure 9). A conceivable explanation might be that water depth here was shallower and zone III subsided later. The drilling at Site 654 on the top of a tilted block (located ~50 km south) revealed at least five intervals of finely laminated gypsum, interbedded with calcareous clay but no thick salt deposits [*Kastens et al*., 1988]. This suggests that the densely spaced high-amplitude reflectors imaged in Figure 9 may be calcareous clay and perhaps some gypsum of upper Messinian age. Their location is close to the N-NE projection of Site 654 onto the line CD and in similar water depth.

Moreover, the thickness of the Pliocene to Holocene cover in zone III is also thinner than at the Sardinia Margin. This may be associated with the greater distance to the sediment source or to the elevation of block B2. The block probably acts as a topographic barrier for sediment transport at least from the west, leading to a reduced sedimentation rate in zone III.

Farther east, from 150 km toward Campania Margin, normal faults offset intrabasement horizon Z and cut the youngest sediment up to the seafloor (Figure 10). Those faults indicate that extensional tectonism was recently still active in the central and eastern region near mainland Italy.

The observations indicate that main extension was first active in the northern and western region and propagated eastward, but some degree of extension started contemporaneously in the entire northern Tyrrhenian. Some of these faults were recently still active in the east, or perhaps they have been reactivated, while tectonic deformation has ceased at the western margin. The migration of the locus of the most important extension from west to east with time is also supported by the existence of deeper subbasins in the west, where extension started somewhat earlier. The recent heat flow of 50 mW/m^2 is typical for a passive continental margin compared to the warmer eastern region with a present heat flow of ~100 mW/m^2 [*Della Vedova et al*., 1984]. A rift migration to the SE is supported by the drilling results of ODP Leg 107 in the central Tyrrhenian Basin [*Kastens et al*., 1988, Sites 654 and 652 in Figure 1], because continental blocks tilted during Tortonian to Messinian age at the upper Sardinia Margin (Site 654) and during Messinian to Pliocene age at the lower Sardinia Margin located farther to the east (Site 652).

5.2. Progressive Crustal Extension

The constraints provided by the data on the timing of rifting, on variations in *Vp* structure, and on the amount of crustal thinning allow us to study the evolution of crustal scale deformation with increasing extension factor and the potential role of synrift magmatism in the northern Tyrrhenian Sea.

Along line AB, the velocity model and rotated fault-bounded blocks show no significant lateral abrupt variations in extension, and the structure appears to have been homogeneously stretched at crustal scale (Figure 3). The amount of extension by brittle faulting is consistent with the stretching factors estimated from the measured crustal thickness, and the overall basin structure is fundamentally symmetric. Indication for W-E rift propagation comes from the flat summits of the blocks A9 and A10 that were recently above sea level and subsided later than blocks at the western margin. Farther west, the Corsica Basin formed during an earlier rifting episode related to the opening of the Ligurian Basin.

Along line CD, rifting at the Sardinia Margin began in late Tortonian, as indicated by dating of sequences drilled at ODP site 654 [*Kastens et al*., 1987], lasting to early Pliocene age, and evidence indicates that the locus on main extension migrated eastward. In spite of the delayed onset of rifting, the central and eastern zones have been stretched the most, to a maximum β factor of 2.2. This factor may be a minimum because the contribution to crustal thickness by rift-related magmatic intrusions or underplating is not well constrained, although based on the *Vp* model, it is probably minor. That important tectonic activity initiated later in zones III and IV suggests that crustal thinning occurred over a shorter period. The presence of the thinnest crust in this area may be explained in two different ways: (1) The extension rate increased in zones III and IV. (2) The extension rate was constant, but the prerift crustal thickness varied laterally.

The first argument appears compatible with the V-shaped geometry of the basin that indicates that the pole of rotation was near the northern sector during rifting and extension rates must have increased southward, although we do not have constraints on potential lateral variations in prerift crustal thickness.

Zone III displays the highest degree of faulting and fracturing along line CD (Figure 6), which is compatible with the ~12% reduction of velocities in this area (Figure 5). Reduced upper crustal velocities, possibly due

to fracturing and alteration, have also been recognized in the Galicia interior basin (offshore west Iberia) associated to decreased fault spacing and block size, as crustal thinning increased [*Pérez-Gussinyé et al*., 2003]. The decrease of the dimension of fault blocks and fault spacing associated with increasing extension factors has also been described from analog modeling [*Ackermann et al*., 2001]. The drilling in the ~3000 m deep Vavilov Basin to the southeast reached serpentinized peridotites near the top basement indicating full continental breakup and mantle exhumation [*Kastens et al*., 1988, Figure 1] and further increased extension south of our study area. Widespread mantle exhumation and serpentinization is supported by seismic data in the area [*Prada et al*., 2014]. The increase of stretching factors and crustal thinning from north to south in the Tyrrhenian Basin shows similarities to the V-shaped Porcupine Basin, west of Ireland. Here the crust is moderately stretched in the north, while the crust in the south is stretched by a factor $>$6, possibly leading to mantle exhumation [*Reston et al*., 2004] and asymmetry. There the asymmetric geometry is inferred by a bright dipping reflection cutting through the basin. This reflection was interpreted as the top of the serpentinized mantle rocks.

Line CD shows that the region of maximum thinning is not located in the basin center. Both the whole crustal thinning and lower crustal thinning of line CD indicate that $>2\,\beta \leq 2.2$ occurs in the eastern portion of zone III (Figure 3) close to the continental shelf of the Italian Peninsula. Although unconstrained by our data, the crust thickens abruptly toward the Peninsula, where it attains ~30 km under the coast line [*Di Stefano et al*., 2011]. Thus, line CD displays a gently asymmetric crustal thinning with respect to the little stretched crust of Sardinia and Italian Peninsula. In the Tyrrhenian Sea, the change from symmetrically stretched crust to an apparently asymmetric configuration is concomitant with the N-S increasing extension rates and eastward migration of the locus of rifting at β factor $>$~2. This might imply a change in the style of tectonic extension. The smaller block sizes and increased faulting of zone III might be related to a second generation of faults that crosscut previous fault-bounded structure, a mechanism known as polyphase faulting [*Reston*, 2005]. This mechanism has also been suggested for the development of the Galicia Margin, but it is difficult to recognize on seismic sections. Polyphase faulting could also be a plausible mechanism for the observations in zone III. It might explain decreasing block size and perhaps the complex structures beneath the postrift cover in the higher extended area where the β factor exceeds ~2. However, the relatively simple rifting history inferred from the synrift sediment infill indicates that faulting occurred mainly on a single, well-defined phase. Strong reflectors, like those observed in the Porcupine Basin and the Iberia Margin, are not evident on our seismic lines and might suggest that faults did not cut the lower crust to allow fluids to serpentinize the upper mantle.

5.2.1. Crustal Thinning

A commonly described feature of rifted margins is that the amount of brittle extension by faulting appears to be less than the amount necessary to explain crustal thinning at stretching factors $>$~2. Some workers explain this discrepancy by different amounts of stretching in the brittle and ductile crustal domains [e.g., *Davis and Kusznir*, 2004] or by slip on crustal scale low-angle normal faults generating wide horizontal extension [*Forsyth*, 1992; *Colletini et al*., 2009]. It has also been proposed that the amount of brittle extension could be strongly underestimated from seismic images due to limited resolution [e.g., *Marrett and Allmendinger*, 1992]; however, it is not enough to explain the thinning at rifted margins [*Reston*, 2007] unless complex crosscutting multiple phases of faulting had occurred [*Reston*, 2005]. Alternatively, thinning, extension, and asymmetry may be explained by focusing on the deformation leading to a change from broadly distributed coeval faulting to faulting occurring sequentially in time at newly formed individual faults [*Ranero and Pérez-Gussinye*, 2010].

Along the less extended line AB, we estimated the amount of brittle extension by analyzing a prestack depth-migrated section and whole crustal thinning using the wide-angle velocity model [*Moeller et al*., 2013]. Our estimation showed that the amount of extension in the upper crust calculated from fault heaves is similar to the measured thinning of the whole crust (Figure 3). Thus, uniform stretching can explain the less extended cross section of the rift basin.

Comparing brittle extension on line CD to whole crustal thinning is more complicated. Syntectonic sedimentary structures in zone III are highly fractured and more difficult to image. This makes the estimation of fault displacement difficult. The comparison of whole crustal thinning to lower crustal thinning shows that the overall lower crust stretching factors match the long-wavelength thinning trend of the whole crust (Figure 3). Obviously, this is based on the assumption that the thickness of

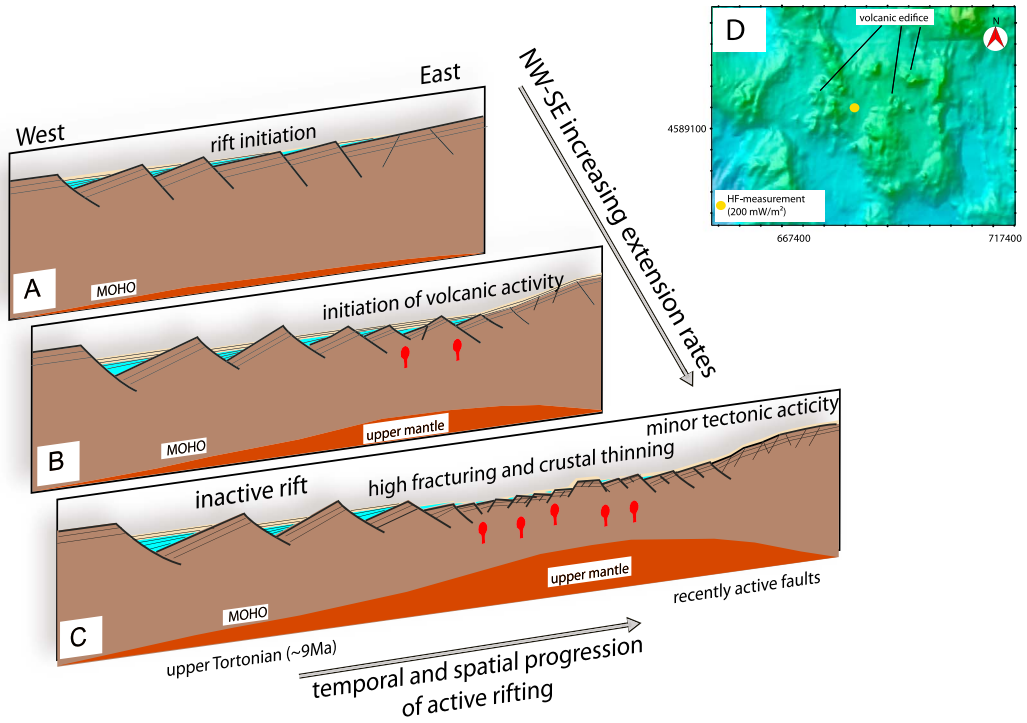

Figure 13. Schematic model for the tectonic evolution of the northern Tyrrhenian Sea Basin. (a) At the beginning of rifting, extension affected the crust just in a narrow region with a few active faults. The crust was thinned uniform by brittle extension and lower crustal flow. (b) Extension rates increase toward the south as the zone of active rifting propagates eastward. This led to a higher stretched zone on a SE orientation, the occurrence of volcanic activity and newly generated young faults in the east. (c) Rifting propagation goes on while the western margin becomes inactive and become covered by postrift sediments. A highly fractured zone developed as a result of increasing extension rate coincides with higher crustal thinning and volcanic activity. Young faults generate at the eastern margin and are to some extent still active. (d) Ring-like structures and pins in the bathymetry data are perhaps related to volcanic edifices. Together with volcanic-related features on both PSTM sections, they are aligned on a NW-SE axis coincident with the axis of increasing stretching factors (see Figure 1a).

the layer between the 6.5 km/s velocity isoline and the Moho represents the lower crust that was stretched by plastic deformation. If this assumption is valid, the upper crust must have been extended by approximately the same amount by brittle faulting, because it has never been observed that brittle faulting is higher than whole crustal extension. Large-scale detachment faults have not been recognized on any of the seismic lines and do not appear to play a role in rift basin formation, at least with extension factors ≤~2.0. Moreover, large displacements on low-angle normal faults, like the Zuccale fault described on Elba Island [*Keller and Coward*, 1996], are not necessary to explain the basin extension at $\beta \leq 2.2$.

In summary, the results indicate that along lines AB and CD, the crust has been stretched homogeneously by a similar amount of brittle extension in the upper crust and ductile deformation in the lower crust. At the maximum β factor, we observe along the southern line (=2.2.) that the overall structure has changed from fairly symmetric to some degree of asymmetry. The thinnest part of the crust in zone III appears to be located more in the eastern part along the line. This zone leads to the southeast over to an area of full continental breakup, the so-called the Vavilov Basin. This process of apparent asymmetry appears to have occurred at $\beta > 1.5 < 2.2$.

5.2.2. Magmatism

Geochronological data have been interpreted to indicate that between Oligocene and recent time, five episodes of magmatic activity affected the Tyrrhenian region [*Savelli*, 1988; Savelli, 2002]. The Oligocene episode affected onshore Sardinia and volcanism is younger toward the east (Figure 1). This volcanic activity migration resembles to the evolution of fault activity and increased crustal thinning toward east deduced from line CD. Seismic images show that magmatic activity is evidently interbedded with sediments of zone III (Figures 9–11). The stratigraphy of line CD indicates a Pliocene age for the sediment containing interpreted

magmatic layers (Figures 9–11). This is similar to the age of an extrusive basaltic flow drilled at Site 654 [*Kastens et al*., 1988]. The age of the interpreted magmatic layers may be younger if they are intrusive sills. The basement high in Figure 10 may have been part of the eruptive system because flows are located west and east of this feature. The subbasin in Figure 11 shows up to three potentially different phases of volcanic activity during Pleistocene age and perhaps late Messinian age. In the vicinity of line CD, volcanic features are not detectable in available bathymetric data of 500 m grid, but in the eastern zone between the profiles, cone-shaped topographic highs may indicate a cluster of volcanoes (Figure 13d). At this location, several heat flow measurements as high as 200 mW/m^2 have been conducted [*Della Vedova et al*., 1984]. The distance from the volcanoes to line CD is 30–40 km so that they may not be related to the layering that is imaged, but it support the magmatic origin. The triangular-shaped basement body with steep flanks buried under postrift sediments (Figure 10) may also represent a volcanic construction. Low-frequency reflections under this feature may be interpreted as volcanic or intrusive layering. The different volcanic features support that a comparatively more robust magmatic activity occurred in the eastern part of the northern Tyrrhenian Basin, perhaps related to the latest phase of extension during rifting progress or slightly postdate tectonism.

The NE-SW alignment of volcanoes visible on bathymetry and interpreted magmatic features on seismic sections correspond spatially to the area of crustal thinning in zone III (Figure 3). Although the generation of magmatism might be a result of thinning and mantle decompression, the eastward decreasing age of volcanic rocks might be related to migration of a volcanic arc, like the Oligocene volcanic rocks onshore Sardinia thought to be arc related [*Cherchi and Montadert*, 1982]. In which way, a moving arc influenced the style of deformation and crustal extension is not clear. Also if the observed magmatism would be rift-related, it remains enigmatic how mantle upwelling and elevated temperatures control rift structures and the style of extension.

The nature of magmatic rock has been previously analyzed using the distribution of velocity with depth. At active intraoceanic arcs or at volcanic passive margins, the *Vp* in the lower crust may range 7–7.5 km/s [*Contreras-Reyes et al*., 2011; *White et al*., 2008] whereas lower continental crust *Vp* ranges from 6.7 to 6.8 km/s [*Christensen and Mooney*, 1995]. Thus, the 6.5–6.7 km/s lower crustal velocity along most of the lines does not support important intrusive magmatism or underplating. The highest lower crustal velocity occurs along line CD 240–300 km, where the crust is the thinnest, and it may perhaps be indicative of minor magmatism, that is spatially coincident with the shallow evidence of volcanic activity observed in the seismic images.

5.3. Tectonic Style

The evolution of a homogeneously stretched crust from a symmetric rift structure to the formation of a crustal scale asymmetry observed in the northern Tyrrhenian Basin may be associated with an increase in the amount of extension of $1.5 < \beta < 2.2$ and associated to a change in faulting style that may be expressed in the highly fractured zone III along line CD. The geometrical evolution of the basin shows apparent similarities to the changes in structure with extension factor at the Porcupine Basin. In the Porcupine Basin, the development of the asymmetry has been proposed to be related to the development of a detachment fault (*P* detachment) possibly associated to the onset of mantle serpentinization when brittle faulting cut the entire crust and water reached the mantle at stretching factors $>$~3 [*Reston et al*., 2004]. In the Tyrrhenian Basin, an apparent asymmetry developed at $1.5 > \beta < 2.2$. In spite of some considerably large-offset faults, a shallow dipping detachment fault is not observed in our data and may not be necessary to control the formation of basin asymmetric structure. The only candidate structure representing a detachment that we have identified is an undulating (in a two-way time section) intrabasement reflection identified e.g., in Figure 12. However, it is unclear what kind of upper crustal deformation it might accommodate. Similar reflections have been interpreted as an Alpine nappe or an Hercynican basement like the "K reflector" in the Tuscany region [*Contrucci et al*., 2005, and references therein]. Our preferred interpretation is that this discontinuous reflection is the Z horizon that has been identified along basically the entire line CD (Figure 6).

5.3.1. Evolutionary Model

The early phases of extension, accompanied by faulting and half graben formation, lead to homogeneous stretching of the entire crust in the Tyrrhenian back-arc basin. This style might be representative of early evolutionary stages of rifted margins. The W-E migration of the locus of main extension with a pole of rotation located near the northern tip of the basin may have controlled the style of faulting, magmatism, and

structural architecture (Figure 13). Rifting began with N-S orientation along the entire western margin, generating large half graben structures at relatively low stretching factors <1.5 (Figure 13 a). When the locus of the main faulting spatially migrated, new faults generated grabens containing relatively younger synrift sedimentary deposits compared to early rifting half grabens synrift deposits. The close location of the pole of rotation implies that extension rates must have increased abruptly toward the south leading to higher stretching factor in the same time span. This extension phase was accompanied by locally focused thinning and extensive faulting creating smaller block sizes (Figure 13b). This effect increased farther south in the basin and leads to small amounts of decompression melting that may locally intrude the lowermost crust and reach the surface in minor volcanic activity (Figure 13c). The extension led to a asymmetric margin configuration with large and inactive half grabens on one margin of the rift and active faults on the other eastern margin (Figure 13c).

6. Conclusions

The study of the northern Tyrrhenian Basin contributes to the basic understanding of extensional processes that lead to continental rifting, basin formation, and development of conjugate margin configurations. We analyzed two coincident wide-angle and prestack time-migrated multichannel seismic lines. This work provides new insights on the crustal architecture and sedimentary units in the northern Tyrrhenian Sea Basin that underwent different amounts of crustal stretching and thinning.

The northern part of the basin opened between upper Tortonian to early Pliocene times. However, we observe that some tectonic activity remains because high-angle normal faults cut the seafloor near the mainland of Italy.

The syntectonic deposits indicate a W-E locus of rifting migration, supporting results from drilling farther south.

Velocity models constrained with wide-angle seismic data, support a little extended, homogeneously thinned crust between the Corsica Basin and the Latium Margin with a flat-lying Moho topography (30% stretching). The system changes to an asymmetric basin configuration between the Sardinia Margin and the Campania Margin and farther to the southeast to full continental breakup in the Vavilov Basin. The 16–19 km thick crust in the west with a stretching factor of 1.3–1.5 grades toward the Campania Margin with 11 km thick crust implying a β factor of 2.2. The change from symmetric to asymmetric rifting occurred at $\beta < 2.2$.

The comparison of crustal thickness variations and faulting supports that stretching is homogeneous across the entire crust. Large-scale detachment features are not necessary to explain the asymmetry of basin structure and no shallow dipping faults have been imaged on PSTM sections.

The zone of the highest β factor, is coincident with a higher degree of faulting. At this site, limited volcanic activity manifested as basaltic layers within postrift sedimentary layers are observed and potential volcanic edifices in the seismic images and bathymetry. The seismic velocity of the lower crust supports that the melts have probably been generated by mantle decompression.

Acknowledgments

A great thank goes to the teams involved in the MEDOC project. We thank the ships' officers and the crews of Spanish R/V *Sarmiento de Gamboa* and Italian R/V *Urania*. Thank you to the UTM and GEOMAR technicians who helped to conduct the data for the MEDOC project successfully. This work was funded by the Deutsche Forschungsgemeinschaft (DFG) under grant GR 1964 /14-1 and the complementary Action OSMART, which has been funded by the Spanish Ministry of Science and Education, with reference CTM2007-66179-C02-01/MAR and CTM2007-66179-C02-02/MAR, and CTM2009-07772-E/MAR, respectively. We thank Grant G. Buffett for grammar editing.

References

Ackermann, R. V., R. W. Schlische, and M. O. Withjack (2001), The geometric and statistical evolution of normal fault systems: An experimental study of the effects of mechanical layer thickness on scaling laws, *J. Struct. Geol.*, *23*, 1803–1819, doi:10.1016/S0191-8141(01)00028-1.

Barker, P. F., and I. A. Hill (1980), Asymmetric spreading in back-arc basins, *Nature*, *285*, 651–654, doi:10.1038/285652a0.

Cherchi, A., and L. Montadert (1982), Oligo-Miocene rift of Sardinia and the early history of the Western Mediterranean Basin, *Nature*, *298*, 736–739, doi:10.1038/298736a0.

Christensen, N. I., and W. D. Mooney (1995), Seismic velocity structure and composition of the continental crust: A global view, *J. Geophys. Res.*, *100*(B6), 9761–9788, doi:10.1029/95JB00259.

Colantoni, P., A. Fabbri, P. Gallignani, R. Sartori, and J. P. Rehault (1981), Carta Litologica e Stratigrafica dei Mari Italiani, Litografia Artistica Cartografica, Firenze.

Collettini, C., A. Niemeijer, C. Viti, and C. Marone (2009), Fault zone fabric and fault weakness, *Nature*, *462*(7275), 907–910.

Contreras-Reyes, E., I. Grevemeyer, A. B. Watts, E. R. Flueh, C. Peirce, S. Moeller, and C. Papenberg (2011), Deep seismic structure of the Tonga subduction zone: Implications for mantle hydration, tectonic erosion, and arc magmatism, *J. Geophys. Res.*, *116*, B10103, doi:10.1029/2011JB008434.

Contrucci, I., A. Mauffret, C. Brunet, A. Nercessian, N. Béthoux, and J. Ferrandini (2005), Deep structure of the North Tyrrhenian Sea from multichannel seismic profiles and on land wide-angle reflection/refraction seismic recording (LISA cruise): Geodynamical implications, *Tectonophysics*, *406*(3–4), 141–163, doi:10.1016/j.tecto.2005.05.015.

Corti, G., and P. Manetti (2006), Asymmetric rifts due to asymmetric Mohos: An experimental approach, *Earth Planet. Sci. Lett.*, *245*(1–2), 315–329, doi:10.1016/j.epsl.2006.02.004, ISSN 0012-821X.

Curzi, P., A. Fabbri, and A. Nanni (1980), The Messinian evaporitic event in the Sardinia Basin area (Tyrrhenian Sea), *Mar. Geol.*, *34*(3–4), 157–170, doi:10.1016/0025-3227(80)90070-5, ISSN 0025-3227.

D'Agostino, N., A. Avallone, D. Cheloni, E. D'Anastasio, S. Mantenuto, and G. Selvaggi (2008), Active tectonics of the Adriatic region from GPS and earthquake slip vectors, *J. Geophys. Res.*, *113*, B12413, doi:10.1029/2008JB005860.

Davis, M., and N. J. Kusznir (2004), *Proc. NSF Rifted Margins Theor. Inst*, edited by G. D. Karner, pp. 92–136, Columbia Univ. Press, New York.

De Franco, R., G. Biella, G. Caielli, A. Mauufret, I. Contrucci, and A. Nercessian (2000), Interpretation of wide angle reflection-refraction data in the Tuscan-Latium peri-Tyrrhenian area, *Bollettino della Societa Geologica Italiana*, *119*, 171–188.

De Luca, L., R. de Franco, G. Biella, A. Corsi, and R. Tondi (2004), An analysis of the first-arrival times picked on the DSS and wide-angle seismic section recorded in Italy since 1968, *Ann. Geophys.*, *47*(6), 1699–1711, doi:10.4401/ag-3369.

Della Vedova, B., G. Pellis, J. P. Foucher, and J.-P. Rehault (1984), Geothermal structure of the Tyrrhenian Sea, *Mar. Geol.*, *55*, 271–289.

Di Stefano, R., I. Bianchi, M. G. Ciaccio, G. Carrara, and E. Kissling (2011), Three-dimensional Moho topography in Italy: New constraints from receiver functions and controlled source seismology, *Geochem. Geophys. Geosyst.*, *12*, Q09006, doi:10.1029/2011GC003649.

Fabbri, A., and P. Curzi (1979), distribution of the Messinian deposits in the Tyrrhenian Sea, *Giornale Geol.*, *43*, 29.

Faccenna, C., T. W. Becker, F. P. Lucente, L. Jolivet, and F. Rossetti (2001), History of subduction and back-arc extension in the Central Mediterranean, *Geophys. J. Int.*, *145*, 809–820, doi:10.1046/j.0956-540x.2001.01435.x.

Forsyth, D. W. (1992), Finite extension and low-angle normal faulting, *Geology*, *20*, 27–30, doi:10.1130/0091-7613(1992)020<0027:FEALAN>2.3.CO;2.

Gawthorpe, R. L., C. A.-L. Jackson, M. J. Young, I. R. Sharp, A. R. Moustafa, and C. W. Leppard (2003), Normal fault growth, displacement localisation and the evolution of normal fault populations: The hammam faraun fault block, suez rift, egypt, *J. Struct. Geol.*, *25*(6), 883–895.

Hsü, K. J., L. Montadert, D. Bernoulli, M. B. Cita, A. Erickson, R. E. Garrison, R. B. Kidd, F. Melieres, C. Müller, and R. Wright (1977), History of the Mediterranean salinity crisis, *Nature*, *267*, 399–403, doi:10.1038/267399a0.

Jolivet, L., D. Frizon de Lamotte, A. Mascle, and M. Seranne (1999), The Mediterranean Basins: Tertiary Extension within the Alpine Orogen – an introduction, *Geol. Soc., London, Special Publ.*, *156*, 1–14, doi:10.1144/GSL.SP.1999.156.01.02.

Kastens, K. A., et al. (1987), Proc. ODP, Init. Repts., 107: College Station, Tex., (Ocean Drilling Program), doi:10.2973/odp.proc.ir.107.1987.

Kastens, K. A., et al. (1988), ODP Leg 107 in the Tyrrhenian Sea: Insights into passive margin and back-arc basin evolution, *Geol. Soc. Am. Bull.*, *100*, 1140–1156, doi:10.1130/0016-7606(1988)100<1140:OLITTS>2.3.CO;2.

Keller, J. V. A., and M. P. Coward (1996), The structure and evolution of the Northern Tyrrhenian Sea, *Geol. Mag.*, *133*, 1–16.

Korenaga, J., W. S. Holbrook, G. M. Kent, P. B. Kelemen, R. S. Detrick, H.-C. Larsen, J. R. Hopper, and T. Dahl-Jensen (2000), Crustal structure of the southeast Greenland margin from joint refraction and reflection seismic tomography, *J. Geophys. Res.*, *105*(B9), 21, 591–21, 614, doi:10.1029/2000JB900188.

Malinverno, A., and W. B. F. Ryan (1986), Extension in the Tyrrhenian Sea and shortening in the Apennines as result of arc migration driven by sinking of the lithosphere, *Tectonics*, *5*(2), 227–245, doi:10.1029/TC005i002p00227.

Marrett, R., and R. W. Allmendinger (1992), Amount of extension on "small" faults: An example from the viking graben, *Geology*, *20*(1), 47–50.

Mauffret, A., Contrucci, C., and Brunet, C. (1999) Structural evolution of the Northern Tyrrhenian Sea from new seismic data. Marine and Petroleum *Geology*, *16*, 5, 381–407, doi:10.1016/S0264-8172(99)00004-5, ISSN 0264-8172.

Medimap (2008), CIESM/Ifremer Medimap Group, Loubrieu B., Mascle J. et al., Morpho-bathymetry of the Mediterranean Sea.

Mele, G., and E. Sandvol (2003), Deep crustal roots beneath the northern Apennines inferred from teleseismic receiver functions, *Earth Planet. Sci. Lett.*, *211*(1–2), 69–78, doi:10.1016/S0012-821X(03)00185-7.

Moeller, S., I. Grevemeyer, C. R. Ranero, C. Berndt, D. Klaeschen, V. Sallares, N. Zitellini, and R. de Franco (2013), Early-stage rifting of the northern Tyrrhenian Sea Basin: Results from a combined wide-angle and multichannel seismic study, *Geochem. Geophys. Geosyst.*, *14*, 3032–3052, doi:10.1002/ggge.20180.

Pérez-Gussinyé, M., and T. J. Reston (2001), Rheological evolution during extension at nonvolcanic rifted margins: Onset of serpentinization and development of detachments leading to continental breakup, *J. Geophys. Res.*, *106*(B3), 3961–3975, doi:10.1029/2000JB900325.

Pérez-Gussinyé, M., C.R. Ranero, T. J. Reston, and D. Sawyer (2003), Mechanisms of extension at nonvolcanic margins: Evidence from the Galicia interior basin, west of Iberia, *J. Geophys. Res.*, *108*(B5), 2245, doi:10.1029/2001JB000901.

Prada, M., V. Sallares, C. R. Ranero, M. G. Vendrell, I. Grevemeyer, N. Zitellini, and R. de Franco (2014), Seismic structure of the Central Tyrrhenian basin: Geophysical constraints on the nature of the main crustal domains, *J. Geophys. Res. Solid Earth*, *119*, 1–19, doi:10.1002/2013JB010527.

Ranero, C. R., and M. Pérez-Gussinye (2010), Sequential faulting explains the asymmetry and extension discrepancy of conjugate margins, *Nature*, *468*, 294–300, doi:10.1038/nature09520.

Reston, T. (2007), Extension discrepany at North Atlantic nonvolcanic rifted margins: Depth-dependent stretching or unrecognized faulting?, *Geology*, *35*, 367–370, doi:10.1130/G23213A.1.

Reston, T. J. (1993), Evidence for extensional shear zones in the mantle, offshore Britain, and their implications for the extension of the continental lithosphere, *Tectonics*, *12*(2), 492–506, doi:10.1029/92TC01564.

Reston, T. J. (2005), Polyphase faulting during the development of the west Galicia rifted margin, *Earth Planet. Sci. Lett.*, *237*(3–4), 561–576, doi:10.1016/j.epsl.2005.06.019.

Reston, T. J., J. Pennell, I. Stubenrauch, I. Walker, and M. Perez-Gussinye (2001), Detachment faulting, mantle serpentinization, and serpentinite- mud volcanism beneath the Porcupine Basin, southwest of Ireland, *Geology*, *29*(7), 587–590.

Reston, T. J., V. Gaw, D. Klaeschen, A. Stubenrauch, and I. Walker (2004), Extreme crustal thinning in the south Porcupine Basin and the nature of the Porcupine Median High: Implications for the formation of non-volcanic rifted margins, *J. Geol. Soc., London*, *161*, 783–798, doi:10.1144/0016-764903-036.

Rosenbaum, G., and G. S. Lister (2004), Neogene and Quaternary rollback evolution of the Tyrrhenian Sea, the Apennines, and the Sicilian Maghrebides, *Tectonics*, *23*, TC1013, doi:10.1029/2003TC001518.

Rosenbaum, G., G. S. Lister, and C. Duboz (2002), Reconstruction of the tectonic evolution of the western Mediterranean since the Oligocene, *J. Virtual Explor.*, *8*, 107–130, doi:10.3809/jvirtex.2002.00053.

Sartori, R. (1990), The main results of ODP leg 107 in the frame of Neogene to recent geology of perityrrhernian areas, in *Proc. ODP, Sci. Results*, vol. 107, edited by K. A. Kastens et al., College Station, Tex., (Ocean Drilling Program).

Sartori, R., G. Carrara, L. Torelli, and N. Zitellini (2001), Neogene evolution of the southwestern Tyrrhenian Sea (Sardinia basin and western Bathyal plain), *Mar. Geol.*, *175*, 47–66, doi:10.1016/S0025-3227(01)00116-5.

Savelli, C. (2002), Time-space distribution of magmatic activity in the western Mediterranean and peripheral orogens during the past 30 ma (a stimulus to geodynamic considerations), *J. Geodyn.*, *34*(1), 99–126, doi:10.1016/S0264-3707(02)00026-1.

Savelli, C. (1988), Late Oligocene to Recent episodes of magmatism in and around the Tyrrhenian Sea: Implications for the processes of opening in a young inter-arc basin of intra-orogenic (Mediterranean) type, *Tectonophysics*, *146*(1–4), 63–181, doi:10.1016/0040-1951(88)90089-3.

Schellart, W. P. (2010), Mount-Etna-Iblean volcanism caused by rollback-induced upper mantle upwelling around the Ionian slab edge: An alternative to the plume model, *Geology*, *38*(8), 691–694.

Selli, R., and F. Fabbri (1971), Tyrrhenian: A Pliocene deepsea. Accademia Nazionale dei Lincei. Rendiconti Classe Scienze Fisiche, *Matematiche Nat.*, *8*, 104–116.

Shillington, D. J., W. S. Holbrook, H. J. A. Van Avendonk, B. E. Tucholke, J. R. Hopper, K. E. Louden, H. C. Larsen, and G. T. Nunes (2006), Evidence for asymmetric nonvolcanic rifting and slow incipient oceanic accretion from seismic reflection data on the Newfoundland margin, *J. Geophys. Res.*, *111*, B09402, doi:10.1029/2005JB003981.

Smith, W. H. F., and D. T. Sandwell (1997), Global seafloor topography from satellite altimetry and ship depth soundings, *Science*, *277*, 1957–1962.

Speckbacher, R., J. H. Behrmann, T. J. Nagel, M. Stipp, and C. W. Devey (2011), Splitting a continent: Insights from submarine high-resolution mapping of the Moresby Seamount detachment, offshore Papua New Guinea, *Geology*, *39*, 651–654, doi:10.1130/G31931.1.

Taylor, B., A. Goodliffe, F. Martinez, and R. Hey (1995), Continental rifting and initial sea floor spreading in the Woodlark Basin, *Nature*, *374*, 534–537, doi:10.1038/374534a0.

Trincardi, F., and N. Zitellini (1987), The rifting of the Tyrrhenian Basin, *Geo Mar. Lett.*, *7*, 1–6, doi:10.1007/BF02310459.

Verschuur, D., P. Hermann, N. Kinneging, C. Wapenaar, and A. Berkhout (1988), Elimnation of surface-related multiply reflected and converted waves, SEG Technical Program, Expanded Abstracts, pp. 1017–1020.

Wernicke, B. (1985), Uniform-sense normal simple shear of the continental lithosphere, *Can. J. Earth Sci.*, *22*, 108–125.

White, R. S., L. K. Smith, A. W. Roberts, P. A. F. Christie, and N. J. Kusznir (2008), Lower-crustal intrusion on the north atlantic continental margin, *Nature*, *452*(7186), 460–464, doi:10.1038/nature06687.

Zelt, C. A., and R. B. Smith (1992), Seismic traveltime inversion for 2-D crustal velocity structure, *Geophys. J. Int.*, *108*, 16–34, doi:10.1111/j.1365-246X.1992.tb00836.x.

Zitellini, N., F. Trincardi, M. Marani, and A. Fabbri (1986), Neogene tectonics of the northern Tyrrhenian Sea, *Giorn. Geol*, *4-8*(1), 2.